Complex multicomponent real-fluid thermodynamic model for high-pressure Diesel fuel injection

C. Rodriguez [a,*], Houman B. Rokni [a,b], P. Koukouvinis [a], Ashutosh Gupta [c], M. Gavaises [a]

[a] *School of Mathematics, Computer Science & Engineering, Department of Mechanical Engineering & Aeronautics, City University London, Northampton Square EC1V 0HB, United Kingdom*

[b] *Afton Chemical Ltd., Bracknell, Berkshire RG12 2UW, UK*

[c] *Afton Chemical Corp., Richmond, VA 23219, USA*

Corresponding author: Carlos.Rodriguez@city.ac.uk

Abstract

The Perturbed-Chain Statistical Associating Fluid Theory (PC-SAFT) has been coupled with Vapor-Liquid Equilibrium (VLE) calculations in a density-based solver of the Navier-Stokes equations to perform multicomponent two-phase simulations of Diesel injections at high-pressure conditions. This molecular-based EoS requires three empirically determined but well-known parameters to model the properties of a specific component, and thus, there is no need for extensive model calibration, as is typically the case when the NIST (REFPROP) library is utilised. PC-SAFT can handle flexibly the thermodynamic properties of multi-component mixtures for which the NIST (REFPROP) library supports only limited component combinations. Moreover, complex hydrocarbon mixtures can be modelled as a single pseudo-component knowing its number averaged molecular weight (MW) and hydrogen-to-carbon (HN/CN) ratio. Published molecular dynamic simulations have been utilised to demonstrate that the developed algorithm properly captures the VLE interface at high-pressure conditions. Several advection test cases and shock tube problems were performed to validate the numerical framework using analytical and exact solutions. Additionally, two-dimensional simulations of n-dodecane and Diesel injections into nitrogen are included to demonstrate the multidimensional, multispecies and multiphase capability of the numerical framework.

Keywords: Subcritical, PC-SAFT EoS, Diesel Fuel Injection

Nomenclature

List of abbreviations

AAD	Average Absolute Deviation
CFD	Computational Fluid Dynamics
CFL	Courant–Friedrichs–Lewy
CPA	Cubic Plus Association
ECN	Engine Combustion Network
ENO	Essentially Non-Oscillatory
EoS	Equation of State
FC	Fully Conservative
GC	Group Contribution

46	HLLC	Harten-Lax-van Leer-Contact
47	HN/CN	Hydrogen-to-Carbon Ratio
48	LES	Large Eddy Simulation
49	MW	Number Averaged Molecular Weight
50	N-S	Navier-Stokes
51	PNAs	Poly-Nuclear Aromatics
52	PR	Peng-Robinson
53	PC-SAFT	Perturbed Chain Statistical Associating Fluid Theory
54	QC	Quasi-Conservative
55	RK2	Second-order Runge–Kutta
56	SAFT-BACK	Boublik-Alder-Chen-Kreglewshi
57	SRK	Soave-Redlich-Kwong
58	SSP-RK3	Third-order strong-stability-preserving Runge–Kutta
59	TPn flash	Isothermal-Isobaric Flash
60	TVD	Total Variation Diminishing
61	TPD	Tangent Plane Distance
62	VLE	Vapor-Liquid Equilibrium
63	WENO	Weighted Essentially Non-Oscillatory
64		

65 *List of Symbols*

66	$\tilde{a}^{res}$	Reduced Helmholtz free energy [-]
67	c	Sound speed [m s^{-1}]
68	d	Temperature-dependent segment diameter [Å]
69	e	Internal energy [J mol^{-1}]
70	h	Enthalpy [J mol^{-1}]
71	g	Gibbs energy [J mol^{-1}]
72	I	Integrals of the perturbation theory [-]
73	k_b	Boltzmann constant [J K^{-1}]
74	m	Number of segments per chain [-]
75	$\bar{m}$	Mean segment number in the system [-]
76	M_M	Molecular weight [g/mol]
77	N_A	Avogadro's number [mol^{-1}]
78	p	Pressure [Pa]
79	p_c	Critical pressure [Pa]
80	R	Gas constant [J mol^{-1} K^{-1}]
81	T	Temperature [K]
82	T_c	Critical temperature [K]
83	x_i	Mole fraction of component i [-]
84	w	Acentric factor [-]
85	Z	Compressibility factor [-]
86		

87 *Greek Letters*

88	β	Overall fraction of vapour phase [-]
89	ε	Depth of pair potential [J]
90	η	Packing fraction [-]
91	ρ	Density [kg/m^3]
92	ρ_m	Total number density of molecules [1/Å^3]

93	σ_d	Segment diameter [Å]
94	θ	Vapour volume fraction [-]
95	φ	Fugacity coefficient [-]
96	μ	Chemical potential [J mol^{-1}]
97		
98	*Superscripts*	
99	*EQ*	Equilibrium
100	*disp*	Contribution due to dispersive attraction
101	*hc*	Residual contribution of hard-chain system
102	*hs*	Residual contribution of hard-sphere system
103	*id*	Ideal gas contribution
104		

1. Introduction

This research is focused on improving the thermodynamic models employed to simulate fuel mixing at elevated pressures. To correctly model the combustion in Diesel engines one needs to characterise the atomisation and mixing of sprays. However, even nowadays these processes are not completely understood. According to the experiments performed by several authors [1]–[5], supercritical mixing exists at pressures near or slightly higher than the critical pressure of the liquid fuel. [6], [7] stated that the convection-diffusion phenomena described by the Navier-Stokes equations governs Diesel engine conditions. More recently, in [8] it was determined that the surface tension remains in effect at the gas–liquid interfaces in ambient conditions slightly above the critical point of the fuel. However, at higher pressure and temperature conditions the surface tension diminishes, as expected for supercritical fuel–air mixtures. Diesel engine operation conditions are considered to be in the diffused controlled mixing regime. In a following study [9], the authors carried out systematic measurements using high-speed long-distance microscopy for three single-component fuels (n-heptane, n-dodecane, n-hexadecane) injected into gas (89.71% N_2, 6.52% CO_2 and 3.77% H_2O) at elevated temperatures (700–1200 K) and pressures (2–11 MPa). The classical evaporation/diffusive mixing boundaries were moved towards higher pressures and temperatures placing Diesel engines conditions in the classical evaporation regime. In [10] the evaporation of n-alkane fuels into nitrogen was investigated at different pressure and temperature conditions carrying out molecular dynamic simulations. The aim of this work was to understand how the transition from classical two-phase evaporation to one- phase diffusion-controlled mixing takes place. Two regimes are identified: (1) subcritical evaporation where a distinctive interface exists separating the liquid core and the ambient gases; and (2) supercritical evaporation where initially the liquid has a surface tension that decreases rapidly and vanishes. In the supercritical evaporation regime, the evaporation rate increases and reaches a maximum after which there is a transition to the supercritical stage. The results obtained have a high degree of agreement against the experimental results obtained by [9].

Numerous simulations of Diesel sprays in the literature exist, which employ Lagrangian methods considering a sharp gas-liquid interface which evolve according to primary and secondary breakup models and evaporation [11]–[13]. However, this configuration presents some limitations to accurately capture dense flow regimes near the nozzle where the liquid fuels disintegrate into ligaments that then form droplets. Moreover, they are sensitive to calibration parameters. In [14], [15] an Eulerian density-based methodology was used to model the primary atomisation of the injected liquid accounting for compressibility effects associated with the high-pressure and injection velocity. A single-phase dense-gas approach was combined

with the Peng-Robinson (PR) EoS. However, n-dodecane/nitrogen mixtures are a TYPE IV mixture, which means that the critical temperature of the mixture is higher than the lower critical temperature of the components and lower than then the higher critical temperature of the compounds. On the other hand, the critical pressure is higher than the critical pressure of the components. Considering that the pressures that can be found in the combustion chamber of Diesel engines are lower than the critical pressure of some nitrogen/fuel mixtures, the VLE state must be included in the simulation. In [16], [17] a multi-species two-phase model for Eulerian large-eddy simulations (LES) was developed. A thermodynamic solver that can compute the properties of a homogenous mixture in supercritical or subcritical states was employed. The LES including VLE thermodynamics of the so-called Spray A benchmark case of the Engine Combustion Network (ECN) performed by [16] shows a high degree of agreement against the available experimental data. Although according to [9], [10] the Spray A ambient conditions (900K, 6MPa) fall in the classic evaporation regime, the authors of [16] justified the use of a diffuse interface due to the high Weber number and low Stokes number. The authors pointed out the issues of employing cubic EoS for modelling hydrocarbon properties at temperatures found inside the injection system [18]–[20]. In [16], due to the 8.6% error when compared to NIST (REFPROP) in the density prediction of n-dodecane at 363K, it was necessary to increase the injection velocity to match the mass-flow measurement leading to an error in the predicted velocity of 50 m/s. These problems could be overcome by applying SAFT models.

The SAFT EoS is based on the perturbation theory, as extensively studied in [21]–[24]. This EoS was developed by [25], [26] applying Wertheim's theory and extending it to mixtures. Each molecule of the mixture is decomposed into spherical segments of equal size forming a repulsive, hard sphere reference fluid. The attractive interactions between segments are included in the model as well as the segment-segment energy needed to form a chain between the hard-sphere fluid segments. If the segments exhibit associative interactions such as hydrogen bonding, a term for this interaction is also included. Among the different variants of the SAFT model, the PC-SAFT is the one implemented here. In this model, hard chains are used as the reference fluid instead of hard spheres. While the SAFT EoS computes segment-segment attractive interactions, the PC-SAFT EoS computes chain-chain interactions, which improves the thermodynamic description of chain-like, fluid mixtures [27]. This molecular-based EoS only requires three empirically determined parameters (when the association term is neglected) to model the properties of a specific component without the need for extensive model calibration. Several publications have highlighted the advantages of the SAFT variants with respect to cubic EoS. [28] shows how the PC-SAFT model presents better results than cubic EoS predicting gas phase compressibility factors and oil phase compressibility. For example, Average Absolute Deviation (AAD) of the gas compressibility factors in the range P=0-1000 bar and T= 0-250 °C for nC_6 are 0.0144 for PC-SAFT, 0.0479 for SRK (applying the Peneloux volume correction) and 0.0425 for PR (applying the Peneloux volume correction). For nC_5, they are 0.0127, 0.0529 and 0.0296 respectively. [29] indicated that the PC-SAFT EoS shows a superior performance to the Cubic Plus Association (CPA) EoS in correlating second order derivative properties, such as speed of sound, dP/dV and dP/dT derivatives, heat capacities and the Joule–Thomson coefficient in the alkanes investigated. The CPA model presents a diverging behaviour in the speed of sound attributed to the wrong description of the dP/dV derivative. Similarly, [30] points out the superiority of the SAFT-BACK (Boublik-Alder-Chen-Kreglewshi) model over the PR EOS. The SAFT-BACK EoS shows reasonable results for the speed of sound in the vapor and liquid phases (AAD% = 2.3%, 2.1%, and 1.8% for methane, ethane, and propane, respectively). However, the results obtained by PR EOS are only similar

188 to measured data at low pressure conditions. The predicted values at high density ranges present
189 an AAD% for methane, ethane, and propane of 28.6%, 14.7%, and 61.2%, respectively.
190 Moreover, in [31] it was shown how cubic EoS predict a linear increase of the Z factor
191 (compressibility factor) with pressure, while the PC-SAFT EoS presents pressure dependence.
192   In [19], the PC-SAFT was used to close the Navier-Stokes equations using both a
193 conservative and a quasi-conservative formulation, where the double flux model of [32]–[34]
194 was applied. It was observed how the conservative formulation generates spurious pressure
195 oscillations while the quasi-conservative scheme presents an error in the energy conservation
196 that produce an unphysical quick heat-up of the fuel. In [18], supercritical injections of Diesel
197 fuel modelled as surrogates comprising four, five, eight and nine components were performed
198 taking advantage of the capacity of the PC-SAFT EoS to flexibly handle the thermodynamic
199 properties of multi-component mixtures. Simulations at affordable CPU times were carried out
200 by reducing the number of times the PC-SAFT EoS is solved by computing the pressure and
201 sonic fluid velocity in the cell centres and performing a reconstruction of these variables at each
202 cell face. This technique was found to smooth-out the spurious pressure oscillations associated
203 with conservative schemes when used along with real-fluid EoS. The novelty in this paper is to
204 present a numerical framework that combines PC-SAFT and VLE calculations in a density-
205 based, fully conservative solver of the Navier-Stokes and energy conservation equations. VLE
206 calculations allow to perform simulations where the fuel enters the combustion chamber at low
207 temperatures (subcritical injections). Published molecular dynamic simulations have been
208 employed to demonstrate that the algorithm properly captures the multicomponent VLE
209 interface at high-pressure conditions. A purely predictive method that employs the PC-SAFT
210 EoS for developing pseudo-components, which are defined to replicate the properties of
211 complex hydrocarbon mixtures (e.g., diesel fuels), has been completed and validated to be used
212 in CFD simulations. Then, complex hydrocarbon mixtures can be modelled as a single pseudo-
213 component knowing its MW and HN/CN ratio. Advection test cases and shock tube problems
214 were performed to validate the numerical framework. Two-dimensional simulations of planar
215 Diesel jets are performed to demonstrate the capability of the developed methodology to model
216 subcritical mixing at high-pressure conditions.
217

2.   PC-SAFT Theory and Methodology

219 In this section it is explained the numerical methodology employed to couple the Navier-Stokes
220 equations, total energy equation, VLE calculations and PC-SAFT model in the same numerical
221 framework. The results of the molecular model and VLE calculations were validated using the
222 experimental results of [45], see Figure 1.
223

2.a. CFD code

225 The Navier-Stokes equations for a non-reacting multi-component mixture containing N species
226 in a x-y 2D Cartesian system have been solved employing the finite volume method. Operator
227 splitting as described in [35] is utilised to separate the hyperbolic and parabolic operators. The
228 global time step is computed using the CFL (Courant-Friedrichs-Lewy) criterion of the
229 hyperbolic part. A thermodynamic solver inspired by the work of [16] is employed to
230 approximate the mixture thermophysical properties by performing PC-SAFT and VLE
231 calculations. To compute the convective fluxes: the conservative variables, pressure and speed
232 of sound are interpolated at the cell faces from cell centres using a fifth-order WENO (Weighted
233 Essentially Non-Oscillatory) scheme [18]; the multicomponent HLLC (Harten-Lax-van Leer-
234 Contact) solver is applied to solve the Riemann problem [36]; and the temporal integration is

carried out using a second-order Runge–Kutta (RK2) method applying the filter presented in [18]. In the parabolic sub-step, linear interpolation is performed for computing the conservative variables, temperature and enthalpy on the cell faces from the corresponding values at the cell centres. The model developed by [37] is used to calculate the dynamic viscosity and the thermal conductivity. Figure 2 shows a schematic representation of the CFD code. See Appendix 1.
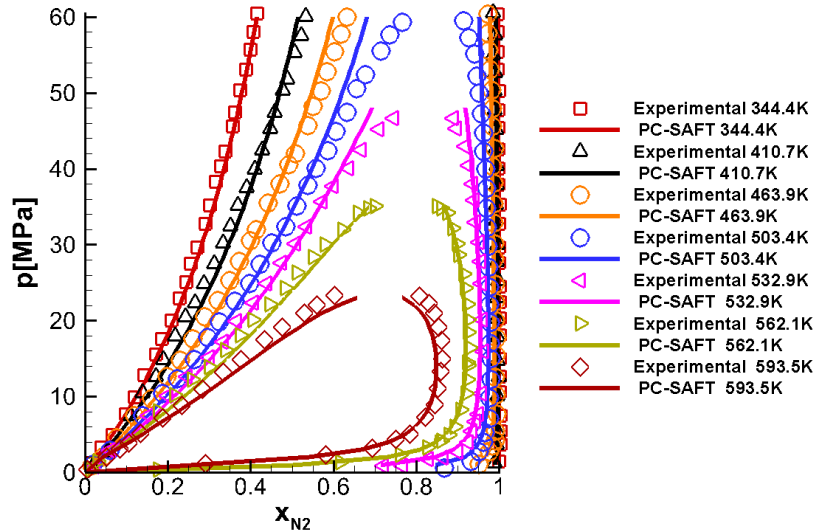
Figure 1. Experimental [38] **and calculated pressure-composition phase diagram for the N_2 (1) + $C_{12}H_{26}$ (2) system. Solid lines: PC-SAFT EoS with kij = 0.144**
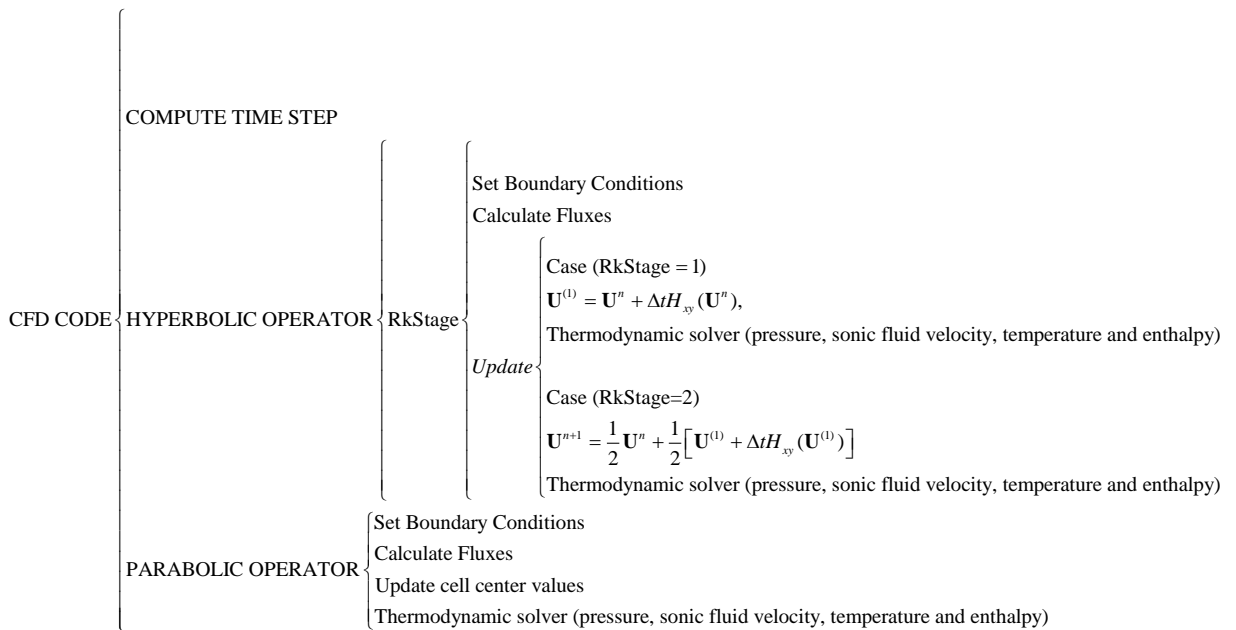
Figure 2. Schematic representation of the CFD code

2.b. Diesel modelling

Two approximations have been considered to model the properties of Diesel.

Multicomponent Diesel surrogates

In [39] four Diesel surrogates have been proposed, divided into two types depending how close their composition is to real Diesel. The V0A and V0B are two low-accuracy surrogates while V1 and V2 are the two higher-accuracy surrogates. Their molar composition is summarized in Table 1. As pointed out in [40], the PC-SAFT EoS shows the highest degree of agreement with the experimental values in comparison with the results obtained using the model developed at NIST [39], see Table 2.

Pseudo-component method

In [41] was developed a technique that defines a single pseudo-component to represent the compounds found in a hydrocarbon mixture. It only requires two mixture properties as inputs, the MW and HN/CN ratio. Here we briefly describe how to achieve the pseudo-component PC-SAFT parameters needed in this study. The group contribution (GC) parameters of [42] are used to develop the correlations shown in Table 4 for n-alkanes and poly-nuclear aromatics (PNAs) that numerically bound the pseudo-component PC-SAFT parameter values. An averaging parameter, Z, is used to calculate the pseudo-component parameters using Eqs. 1-3. Eqs 4-7 show that Z is calculated using the mixture MW and HN/CN ratio, which can be directly calculated knowing the mixture components or can be obtained using elemental analysis for unknown mixtures. Considering that the PC-SAFT is implemented using loops that depend on the number of components solved, this method allows us to model complex hydrocarbon mixtures as one component, thus, reducing significantly the computational requirements of the simulation but with increasing its accuracy.

Table 1. PC-SAFT pure component parameters [40], [42]

Compound	m	σ (Å)	ε/k (K)
n-hexadecane	6.669	3.944	253.59
n-octadecane	7.438	3.948	254.90
n-eicosane	8.207	3.952	255.96
heptamethylnonane	5.603	4.164	266.46
2-methylheptadecane	7.374	3.959	254.83
n-butylcyclohexane	3.682	4.036	282.41
1,3,5-triisopropylcyclohexane	4.959	4.177	297.48
trans-decalin	3.291	4.067	307.98
perhydrophenanthrene	4.211	3.851	337.52
1,2,4-trimethylbenzene	3.610	3.749	284.25
1,3,5-triisopropylbenzene	5.178	4.029	296.68
tetralin	3.088	3.996	337.46
1-methylnaphthalene	3.422	3.901	337.14

Table 2 Comparison between experimentally measured surrogate densities (kg/m³) at 293.15 K and 0.1 MPa with the NIST and PC-SAFT predictions

Surrogate	Experiment[39]	NIST	PC-SAFT
V0A	818.0	809.1	814.9
V0B	837.5	821.6	833.2
V1	828.4	814.1	825.2
V2	853.0	839.9	861.8

The methodology developed by [41] was validated for modelling density, isothermal compressibility and volumetric thermal expansion coefficient of hydrocarbon mixtures, jet and diesel fuels. However, the pseudo-component must correctly model the internal energy (employed in the conservation of the total energy equation) speed of sound (used to calculate the hyperbolic fluxes and time step), enthalpy (employed in the parabolic operator of the Navier-Stokes equations) and fugacity coefficients (to perform VLE calculations). Using the PC-SAFT, the internal energy, enthalpy and heat capacities at constant pressure and volume (needed to compute the speed of sound) are computed as the sum of ideal and residual contributions. The PC-SAFT pure component parameters obtained employing the method of [41] are used to calculate the residual contributions. The ideal enthalpy of each component is calculated by integrating the ideal heat capacity at constant pressure with respect to temperature [43]. The molar composition of the mixture is used to calculate the ideal enthalpy of the mixture. The ideal internal energy of the mixture is computed employing the ideal enthalpy of the mixture. The ideal heat capacities at constant pressure of each component is computed employing the correlations published in [43]; then, molar fractions are used to compute the ideal heat capacity at constant pressure of the mixture, which is employed to calculate the ideal heat capacity at constant volume.

Table 3. Molar composition for the four Diesel fuel surrogates (V0A, V0B, V1, V2) [39]

Compound	V0A	V0B	V1	V2
n-hexadecane	27.8	-	2.70	-
n-octadecane	-	23.5	20.2	10.8
n-eicosane	-	-	-	0.80
heptamethylnonane	36.3	27.0	29.2	-
2-methylheptadecane	-	-	-	7.3
n-butylcyclohexane	-	-	5.10	19.1
triisopropylcyclohexane	-	-	-	11.0
trans-decalin	14.8	-	5.50	-
perhydrophenanthrene	-	-	-	6.00
1,2,4-trimethylbenzene	-	12.5	7.5	-
1,3,5-triisopropylbenzene	-	-	-	14.7
tetralin	-	20.9	15.4	16.4
1-methylnaphthalene	21.1	16.1	14.4	13.9

$$m_{\text{pseudo} - \text{component}} = (1 - Z)m_{\text{n} - \text{alkane}} + Zm_{\text{PNA}} \tag{1}$$

$$(m\sigma)_{\text{pseudo} - \text{component}} = (1 - Z)(m\sigma)_{\text{n} - \text{alkane}} + Z(m\sigma)_{PNA} \tag{2}$$

$$\left(\varepsilon/k\right)_{\text{pseudo} - \text{component}} = (1 - Z)\left(\varepsilon/k\right)_{\text{n} - \text{alkane}} + Z\left(\varepsilon/k\right)_{\text{PNA}} \tag{3}$$

$$Z = \begin{cases} \frac{\text{DoU}_{\text{mixture}}}{\text{DoU}_{\text{PNA}}}, & \text{MW}_{\text{mixture}} < 178 \text{ g/mol} \\ \frac{\text{DoU}_{\text{mixture}}}{10}, & \text{MW}_{\text{mixture}} \geq 178 \text{ g/mol} \end{cases} \tag{4}$$

$$\text{DoU}_{\text{PNA}} = 0.05993 \times \text{MW} - 0.68158 \tag{5}$$

$$CN_{mixture} = \frac{MW_{mixture}}{12.01 + 1.01\left((HN/CN)_{mixture}\right)} \tag{6}$$

$$DoU_{mixture} = \frac{1}{2}\left(2 \times CN_{mixture} + 2 - HN_{mixture}\right) \tag{7}$$

Table 4. PC-SAFT parameter correlations as a function of MW (g/mol) for n-alkanes and PNAs using the GC parameters of [42]

	n-alkane	PNA
m	$0.0274MW + 0.4648$	$0.0163MW + 0.9256$
$m\sigma$ (Å)	$0.1092MW + 1.5677$	$0.0612MW + 3.5324$
ε/k (K)	$\exp(5.5811 - 10.2507/MW)$	$\exp(5.5657 - 8.6620/MW)$

2.c. Thermodynamic solver (PC-SAFT + VLE)

The thermodynamic solver is employed to compute temperature, pressure, sound speed and enthalpy once the conservative variables have been updated. The inputs are the density, internal energy and mass fraction of the components. Three pure component parameters per compound (number of segments per chain, energy parameter and segment diameter) are specified for initialisation. Only an overview of the method is included in this section.

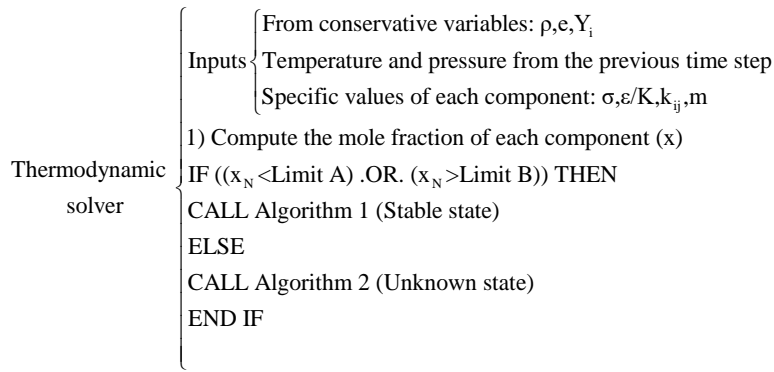**Algorithm**

The algorithm is summarized in Figure 3. The main steps are:

1) **Filter**. This step is employed to decrease the computational time by reducing VLE calculations. By checking the molar fractions of the components, it can be determined whether only one phase exists. Isobaric-adiabatic lines can be computed using the initial conditions of the case of interest (temperature in the chamber, temperature of the fuel and pressure in the combustion chamber) to determine the molar fractions at which VLE is not expected. For example, as we can see in Figure 4, by performing an injection of n-dodecane at 363K in a combustion chamber at 900K and 11MPa, the nitrogen mole fraction at which the fuel starts vaporizing is close to 0.15 and there is not liquid phase at nitrogen mole fractions higher than 0.95 . In this case, it would be safe to consider that any mixture with a nitrogen molar fraction lower than 0.05 (Limit A) and higher than 0.95 (Limit B) will not be in a VLE state. The reason of choosing a low Limit A is to consider the pressure variations along the simulation, which have an important effect on the stability of n-dodecane / N2 mixtures.

2) **Stable state (one phase).** When knowing that the mixture is stable the molecular density of the mixture can be computed and used as an input to the PC-SAFT model. A Newton method is employed to compute the temperature that is needed to calculate the value of all other thermodynamic variables. The temperature dependent function used in the iterative method is the internal energy. The derivative of the internal energy with respect to the temperature at constant molecular density can be directly obtained as these are the independent variables of the PC-SAFT model. See Appendices 2 and 3.

```
                    ┌     ┌ From conservative variables: ρ,e,Y_i
                    │ Inputs ┤ Temperature and pressure from the previous time step
                    │     └ Specific values of each component: σ,ε/K,k_ij,m
                    │ 1) Compute the mole fraction of each component (x)
 Thermodynamic      ┤ IF ((x_N <Limit A) .OR. (x_N >Limit B)) THEN
   solver           │ CALL Algorithm 1 (Stable state)
                    │ ELSE
                    │ CALL Algorithm 2 (Unknown state)
                    │ END IF
                    └
```

Figure 3. Schematic representation of the thermodynamic solver
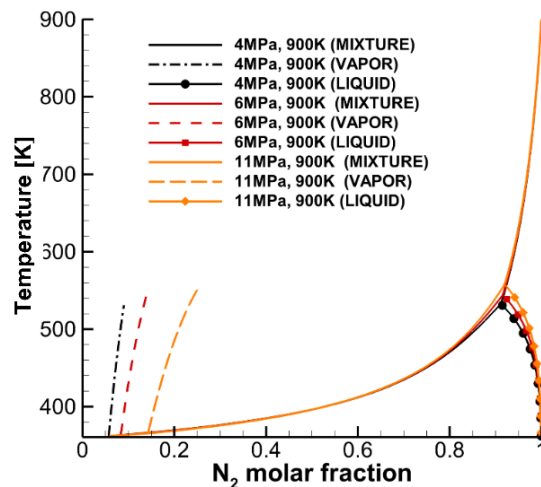
Figure 4. Isobaric-adiabatic mixing lines (N2 + C12H26) at different pressures in the combustion chamber

3) **Unknown state.** If the state of the mixture is unknown the density cannot be used as an input. The pressure and the temperature are iterated employing a multidimensional Newton method until the density and the internal energy obtained using the PC-SAFT + VLE calculations are the ones obtained from the conservative variables. For each P-T calculation a stability analysis is performed to determine if the mixture is stable. See Appendices 4 and 5.

    a. **Mixture stable:** The PC-SAFT model is solved. The reduced density is iterated until the computed pressure is the input pressure.

    b. **Mixture unstable:** The isothermal-isobaric flash problem (TPn flash) is solved and the properties of the fluid in a VLE state are computed.

Stability analysis

A mixture is stable at a specific T and P if the total Gibbs energy is at its global minimum. If an infinitesimal amount (δe) of a new phase of composition **w** is formed from a phase of composition **z,** the change in the Gibbs energy can be expressed as [44]:

$$\delta G = \delta e \sum_{i=1}^{C} w_i(\mu_i(\boldsymbol{w}) - \mu_i(\boldsymbol{z})) \tag{8}$$

381 μ being the chemical potential.

382

383 A necessary condition for the stability of the phase of composition $\mathbf{z}$ is that δG is non-negative
384 for any positive δe for any composition $\mathbf{w}$. This is known as the tangent plane condition of
385 Gibbs.

386 $$\sum_{i=1}^{C} w_i(\mu_i(\mathbf{w}) - \mu_i(\mathbf{z})) \geq 0 \quad \forall \quad w_i \geq 0 \quad \text{such that} \quad \sum_{i=1}^{C} w_i = 1 \qquad (9)$$

387

388 The Tangent Plane Distance (TPD) function [45] is employed to determine if a split into two
389 phases decreases the Gibbs energy.

390 $$TPD(\mathbf{w}) = \sum_{i=1}^{C} w_i(\mu_i(\mathbf{w}) - \mu_i(\mathbf{z})) \qquad (10)$$

391 The TPD function can be written in a dimensionless form employing the fugacity coefficient
392 (φ):

393 $$tpd(w_i) = \frac{TPD}{RT} = \sum_{i=1}^{C} w_i[ln\varphi_i(\mathbf{w}) + lnw_i - d_i(\mathbf{z})] \qquad (11)$$

394 being
395 $$d_i(\mathbf{z}) = ln\varphi_i(\mathbf{z}) + lnz_i$$

396

397 The mixture of composition $\mathbf{z}$ is considered stable if all the TPD local minima are non-negative.
398 $$tpd(\mathbf{w}) \geq 0 \quad \forall \quad w_i \geq 0 \quad \forall \quad w_i \geq 0 \quad \text{such that} \quad \sum_{i=1}^{C} w_i = 1 \qquad (12)$$

399

400 The Successive Substitution Iteration (SSI) algorithm ([16], [46]) (without the Newton
401 method) has been employed to determine if the mixture is stable. See Appendix 6.

402

403 **TPn flash**
404 Once it is known that the mixture is in a VLE state, a multidimensional Newton iteration in T
405 and P is performed until the internal energy and density of the liquid-gas mixture are the ones
406 determined by the conservative variables. An isothermal-isobaric flash problem (known as TPn
407 flash) is performed for each iteration.

408

409 A necessary condition for equilibrium is that the chemical potential for each component is the
410 same in the liquid and vapor phases.
411 $$\mu_i^L = \mu_i^V \qquad (13)$$
412 or equivalently using the fugacities:
413 $$f_i^L = f_i^V \qquad (14)$$

414

415 Employing the fugacity coefficients, this expression can be written as:
416 $$F_i = ln\varphi_v(T, p, y) - ln\varphi_l(T, p, x) + lnK_i = 0 \qquad (15)$$
417 where
418 $$K_i = \frac{x_i}{y_i} = \frac{\varphi_{i,l}}{\varphi_{i,v}} \qquad (16)$$

419

420 A successive substitution method is employed to perform equilibrium calculations at specified
421 temperature, pressure and overall composition to determine the liquid and vapor phases that
422 satisfy eq.15 [16], [44]. See Appendix 7.

423

424

2.d. VLE interface

In [10], molecular dynamic simulations of three n-alkane fuels into nitrogen under various temperatures and pressures were performed to study the injection, evaporation and mixing processes of hydrocarbon fuels into a supercritical environment. The study was focused on understanding the transition from classical two-phase evaporation to one-phase diffusion-controlled mixing. Using as threshold a dimensionless transition time (the time needed to transit from subcritical to supercritical respect to the liquid lifetime) of 0.35, the authors identified two regions on the P-T diagram, see Figure 5. Supercritical dominated: Due to the high critical pressures of TYPE IV mixtures, a VLE state is present at the beginning of the evaporation process. The temperature of the liquid core goes up until the VLE state disappears and only a diffusion-controlled mixing process exists. Subcritical dominated: A clear interface exists between the liquid core and the ambient gases. Nitrogen is not able to diffuse into the liquid core (constant fuel mass fraction close to 1 during evaporation, see Figure 7). There is a gradual decrease of the density of the liquid core as the fuel is heated-up. The evaporation reaches a constant state with a constant liquid core.

According to the classification presented by [10], the combustion chamber of a Diesel engine working at medium-high load operation conditions is in the supercritical dominated regime after the compression cycle, see Figure 5. At these ambient conditions, the nitrogen is able to rapidly diffuse into the liquid core indicating that the interface has a Knudsen-number low enough to fall within the fluid mechanic continuum domain [7]. At 20MPa, the molar fraction of nitrogen in the liquid core (before the transition to a diffusion-controlled mixing process) at 0.5ns is almost 20%, see Figure 6. Therefore, the heat-up of the liquid core is dominated by diffusion phenomena. This can be proven by showing how isobaric-adiabatic mixing lines can replicate the heat-up profiles obtained in the molecular simulations of [10]. The isobaric-adiabatic lines where computed using eq.17. Figure 7 clearly shows how this hypothesis is not applicable in the subcritical dominated regime where after 5 ns the N_2 molar fraction in the liquid core has a constant value of 2%.

$$h_{mixture} = y_{C_{12}H_{26}} h_{C_{12}H_{26}} + y_{N_2} h_{N_2} \tag{17}$$
$$p = 20 MPa$$

being y the mass fraction.

The hypothesis employed in this paper is that the vaporization process at high-pressure Diesel fuel injections is located at the subcritical vaporization stage of the supercritical vaporization regime described by [10] without a transition to the diffusion-controlled mixing process. Being the convective forces much more dominant than the diffusion phenomena, N_2-n-dodecane mixing takes place in a time several orders of magnitude lower than the one observed in Figure 6 where only diffusion is present. Thus, the heat-up of the jet describes a single isobaric-adiabatic mixing line instead of multiple adiabatic lines at different times. This can be corroborated observing the results obtained by [15], [16] where the heat-up of the heat follows an isobaric-adiabatic mixing line constant in time solving both, convection and diffusion phenomena in their simulations. A diffuse interface method, which describe an adiabatic heat-up of the jet, must be applied during Diesel engine injection simulations at high-pressure conditions (supercritical dominated regime) to properly characterize how the fuel vaporize.
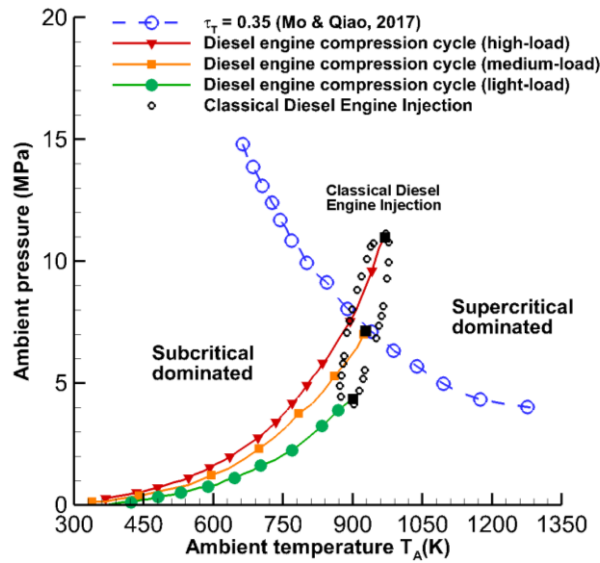
Figure 5. Diesel engine compression cycles [15] **and contours of dimensionless transition time on pressure-temperature diagram of n-dodecane** [10]
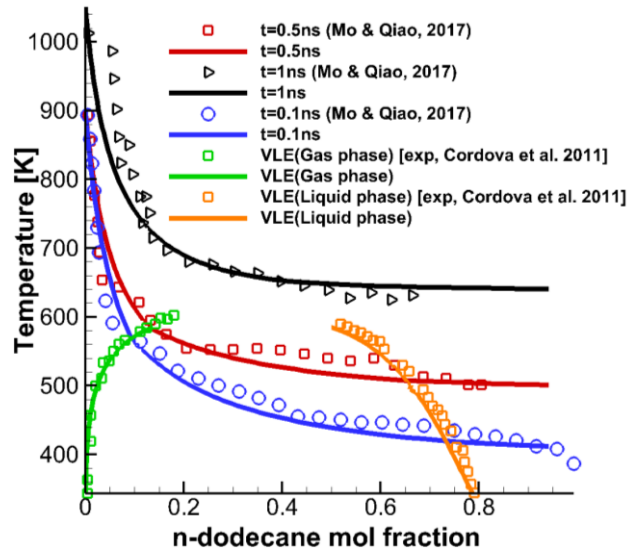
Figure 6. Development of gas–liquid interface shown on VLE diagram at 20 MPa [10]**, VLE experimental data** [38] **and isobaric-adiabatic mixing lines.**

3. Results

The working fluids employed are the following: (i) n-dodecane, (ii) a mixture of n-octane, n-dodecane and n-hexadecane; (iii) a pseudo-component that replicate the properties of the previous mixture; (iv) V0A Diesel, and (v) a pseudo-component that replicate the properties of the V0A Diesel.

3.a Shock Tube Problems

Shock Tube Problem 1 (One phase, one component)

A shock tube problem is used to validate the numerical solution of the hyperbolic operator. The results are compared with an exact solution computed using the methodology described in [47].
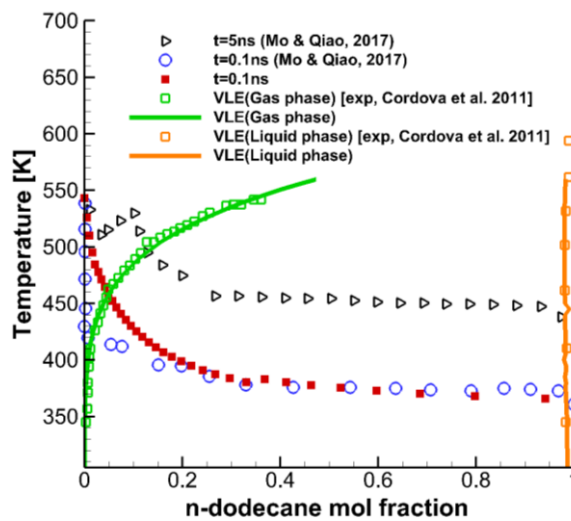
13

489 N-dodecane is utilized as working fluid; the domain is x ∈ [-0.5, 0.5] m; 300 equally spaced
490 cells were employed; wave transmissive boundary conditions are used in the left and right sides;
491 the simulated time is 5 10^{-4}s; the initial conditions in the left state are ρ_L=438kg/m^3, p_L= 30MPa,
492 u_L=0m/s; and in the right state are ρ_R=100kg/m^3, p_R=10MPa, u_R=0m/s. Figure 8 shows how the
493 density, temperature, velocity and pressure results agree with the exact solution.
494
495 **Shock Tube Problem 2 (One phase, multicomponent/pseudo-component)**
496 The working fluids employed are a mixture of n-octane, n-dodecane and n-hexadecane (Table
497 5) and a pseudo-component that replicate the properties of the mixture (Table 6) [41]. Figure 9
498 shows a comparison of the results obtained employing the multicomponent mixture and the
499 results obtained by [41].
500

501
502 **Figure 7. Development of gas–liquid interface shown on VLE diagram at 1 MPa** [10]**, VLE**
503 **experimental data** [38] **and isobaric-adiabatic mixing line.**
504
505 The domain is x ∈ [-0.5, 0.5] m; 800 equally spaced cells were employed; wave transmissive
506 boundary conditions are used in the left and right sides; the simulated time is 5 10^{-4}s; the initial
507 conditions in the left state are ρ_L=438kg/m^3, t_L= 859.5K, u_L=0m/s; and in the right state are
508 ρ_R=100kg/m^3, t_R=1744K, u_R=0m/s. Figure 10 presents the density, temperature, pressure,
509 velocity, speed of sound and internal energy results. The pseudo-component results are the
510 same as the multicomponent ones indicating that the methodology developed by [41] can be
511 used to model complex hydrocarbon mixtures as a pseudo-component in CFD simulations that
512 present one phase.
513
514
515 **Table 5. Molar composition of hydrocarbon mixture employed in Shock Tube Problem 2** [41]

Compound	Hydrocarbon mixture (Molar composition)
n-hexadecane	0.232
n-octane	0.460
n-dodecane	0.232

516
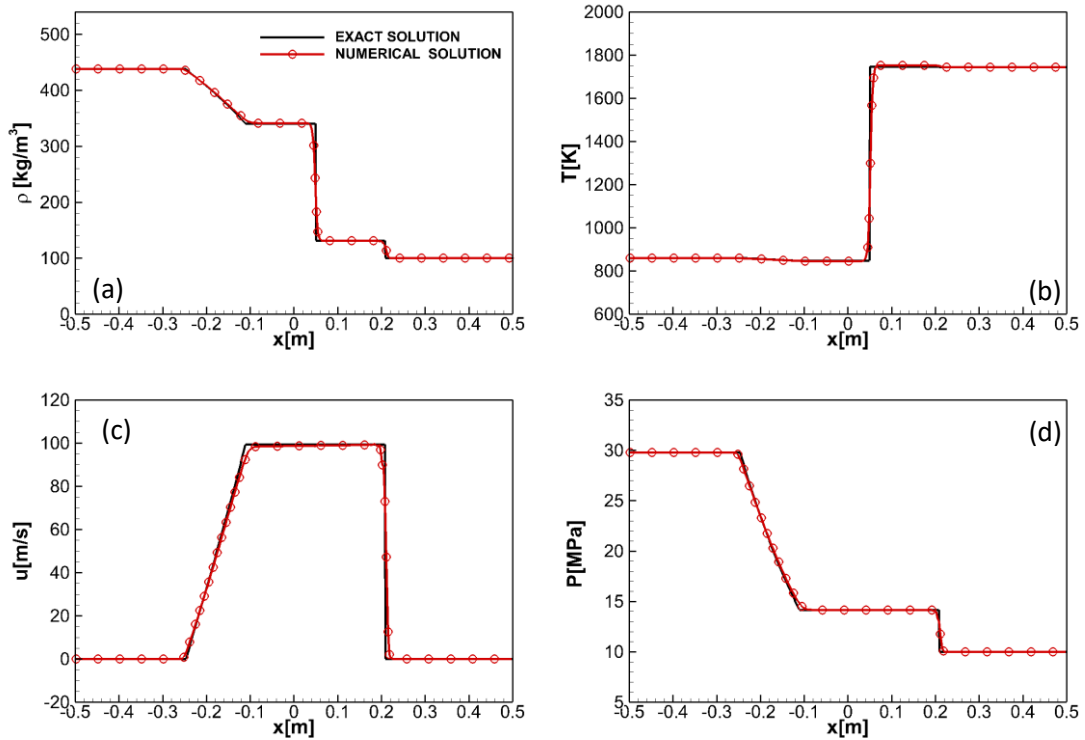
Figure 8. Shock Tube Problem ($C_{12}H_{26}$). CFL = 0.5, u = 0 m/s, 300 cells, t=5 10^{-4} s. Comparisons of (a) density, (b) temperature, (c) velocity and (d) pressure profiles: exact solution and numerical solutions.
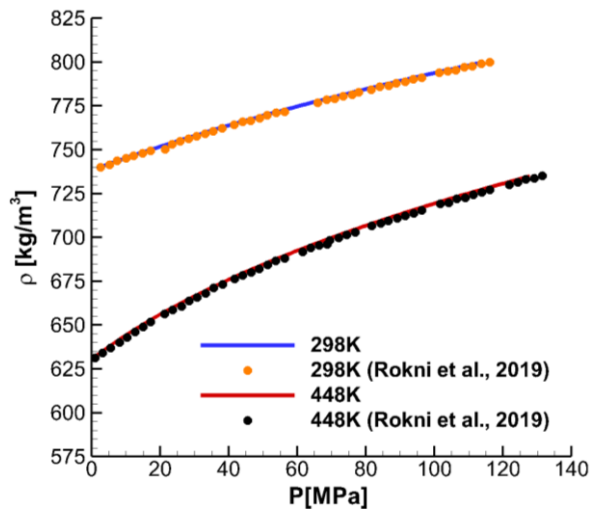
Figure 9. Density predictions for the hydrocarbon mixture presented in Table 5.

Table 6. PC-SAFT pure component parameters employed to model the pseudo-component employed in Shock Tube Problem 2 [41]

Compound	m	σ (Å)	ε/k (K)
Pseudo-component	7.387	3.400	234.47

15

3.b Advection test cases

The computational domain is x ∈ [-10^-5, 10^-5] m; the simulated time is 10^-6s; the left initial conditions are fuel at p=11MPa, u=10.0m/s and t=362K; the right initial conditions are nitrogen at p=11MPa, u=10.0m/s and t=972K; a uniform grid spacing (100 cells) is applied; CFL is set to be 0.5; wave transmissive boundary conditions are implemented in the left and right sides of the computational domain; and a smooth initial interface is applied to reduce the initial start-up error [48]. When a diffuse interface method is employed, the interfaces are not sharp one-point jumps but smooth as they are resolved [48]. Thus, a smooth initial profile is a realistic initial condition. The initial interface was computed employing eq.18 [16] .

$$Y_{FUEL} = 0.5 - 0.5erf\{(x_1 + 0.25l_{ref})/(0.01l_{ref})\} \tag{18}$$

The initialization of each cell located in the interface is performed knowing the pressure, enthalpy of the mixture (eq.17) and the molar fraction of the components.
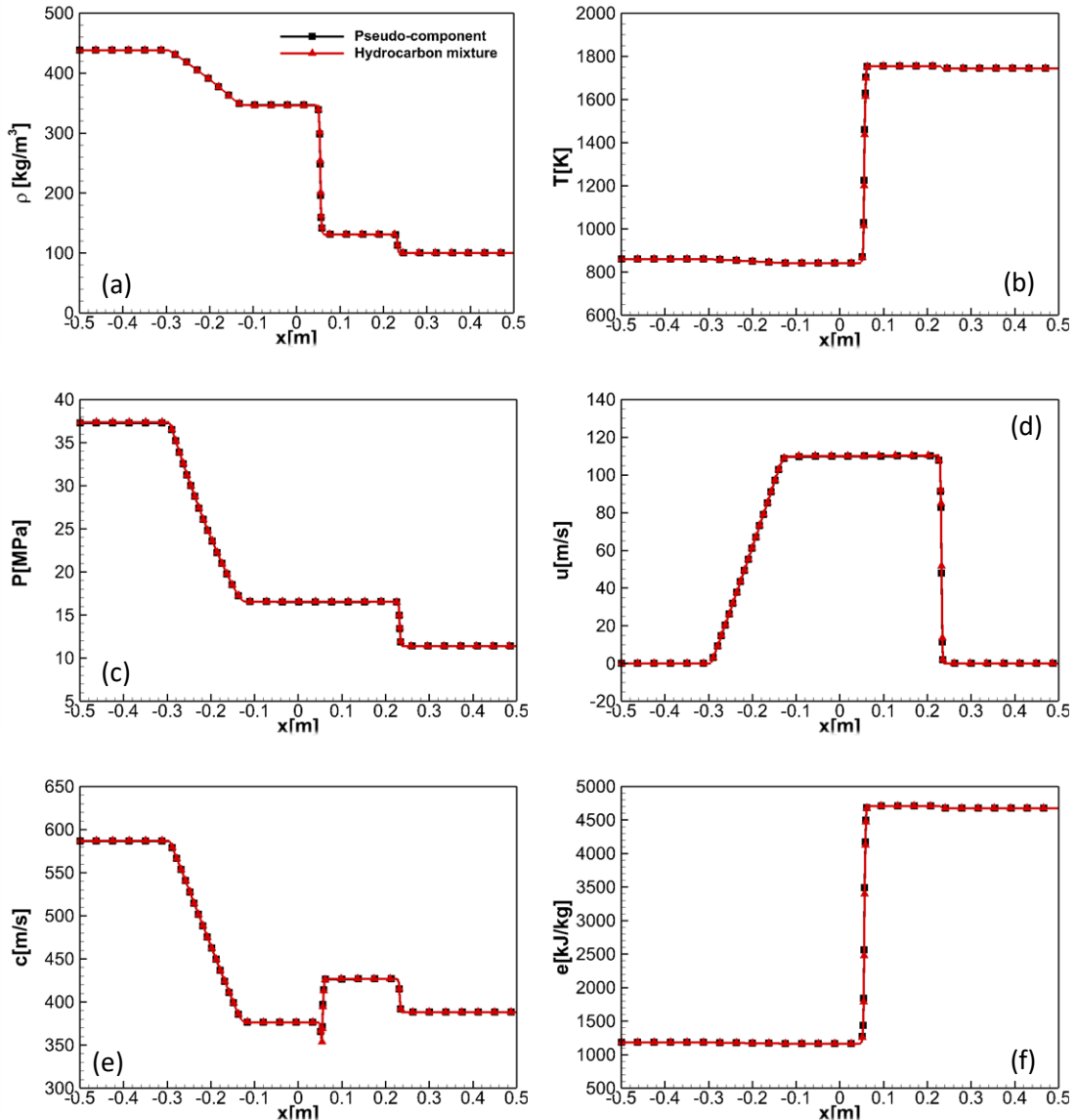
Figure 10. Shock Tube Problem 2. CFL = 0.5, 800 cells, t=5 10^-4 s. Comparison of the (a) density, (b) temperature, (c) pressure, (d) x-velocity, (e) sonic fluid velocity, (f) internal energy using as working fluids are a mixture of n-octane, n-dodecane and n-hexadecane (Table 5) and a pseudo-component that replicate the properties of the mixture (Table 6) [41].

548 **Advection test cases 1 (Two phases, n-dodecane/nitrogen)**

549   Figure 11 shows the results of this advection test case where n-dodecane is employed
550 as fuel. The binary interaction parameter applied is k_{ij} = 0.1446. The numerical framework
551 perfectly captures the large density and temperature gradients present in this multicomponent-
552 multiphase one-dimensional test case. Small spurious pressure oscillations appear in the
553 solution. This problem is well known in multicomponent density based codes employing highly
554 non-linear EoS [16], [19], [33]. Although the small oscillations in the pressure field could be
555 avoided or reduced employing a QC formulation like the double flux model [32]–[34] or using
556 a pressure evolution equation [16], [49], [50] instead of the total energy conservation equation
557 , these schemes presents an error in the energy conservation that produce an unphysical quick
558 heat-up of the fuel [16], [51]. The combination of VLE + PC-SAFT calculations allows to
559 properly model: (1) the properties of n-dodecane at high density ranges where cubic models
560 show large deviations in the sonic fluid velocity (used in density based CFD codes to compute
561 the hyperbolic fluxes and time step [19]), temperature and internal energy; (2) and a correct
562 (adiabatic) subcritical evaporation process in the interface (Section 2.d).
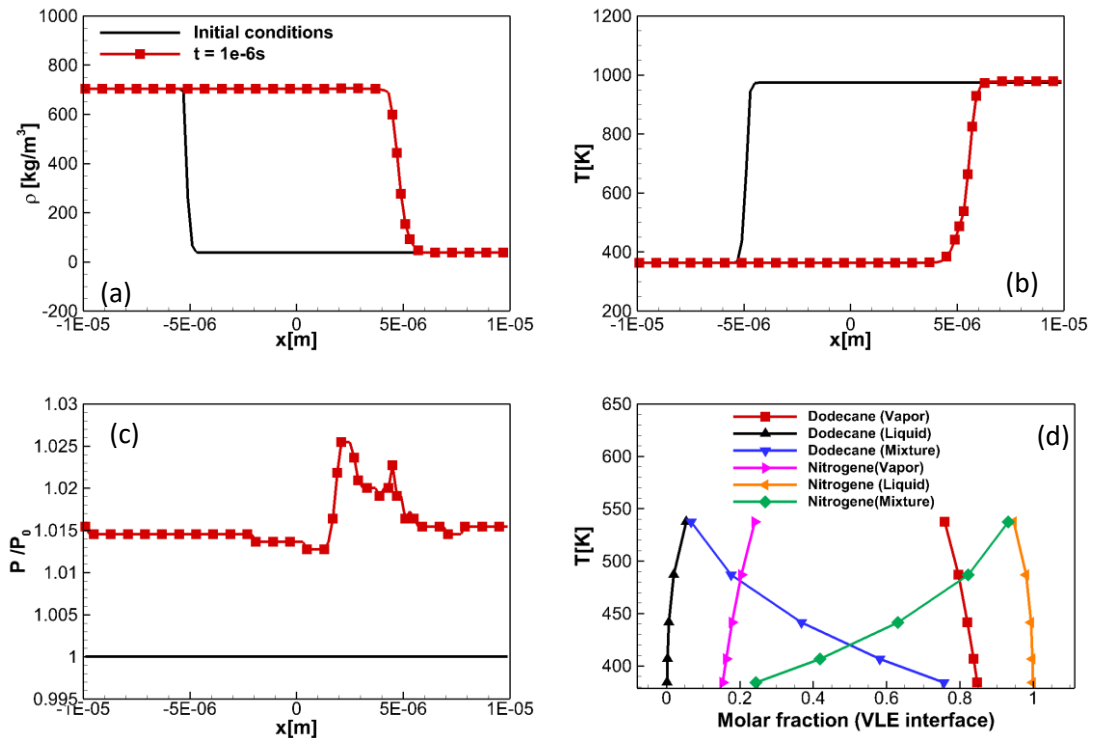
563   **Figure 11. Advection Test Case 1 (N_2- $C_{12}H_{26}$), CFL = 0.5, u = 10 m/s, 100 cells. Results of**
564   **(a) density, (b) temperature, (c) pressure and (d) VLE interface at 10^{-6}s.**

565

566 **Advection test case 2 (Two phases, V0A Diesel/ nitrogen, pseudo - V0A Diesel / nitrogen)**

567   Figure 12 shows the temperature, density, speed of sound and internal energy results of
568 an advection test case that employs the multicomponent Diesel V0A and the pseudo-Diesel
569 V0A (Table 7) as fuels. The binary interaction parameter used between the nitrogen and the
570 Diesel compounds or the pseudo-component is the same one used in the N_2 / n-dodecane
571 mixture (kij = 0.1446). The pseudo-component presents an error (using as reference the
572 multicomponent Diesel results) of 1.6% in density, 3.7% in sonic fluid velocity and 5.5% in
573 internal energy. However, the computational time required to solve the multicomponent V0A
574 Diesel advection test case is 432% the time consumed by the pseudo-Diesel advection test case.
575 The different computational requirements will be even bigger in multidimensional cases or

576 simulations where the hydrocarbon mixture presents more components (e.g., V0B, V1 and V2
577 Diesel surrogates). In the case of the Diesel surrogate V0a, the equilibrium state of five
578 components must be computed in each cell of the interface, see Figure 13. Using the
579 methodology of [41], the number of working fluids is limited to 2 (pseudo-Diesel + N_2).

580   Figure 14 shows how the phase boundary from VLE at 11MPa is different if the
581 multicomponent Diesel V0A or its pseudo-component are employed. The use of a pseudo-
582 component must not alter how the fuel is heat-up, especially in Diesel injection simulations
583 where the temperature plays a significant role on determining the ignition time. Figure 15
584 presents the results in the VLE interface of both working fluids (multicomponent mixture and
585 pseudo-component).

586
587

588 **Table 7. Pseudo-component PC-SAFT parameters employed to model the pseudo-Diesel V0A**
589   **using the correlations developed by utilizing the GC parameters of Tihic et al.** [42]

Compound	m	σ (Å)	ε/k (K)
Pseudo-component	5.436	3.908	256.700

590
591
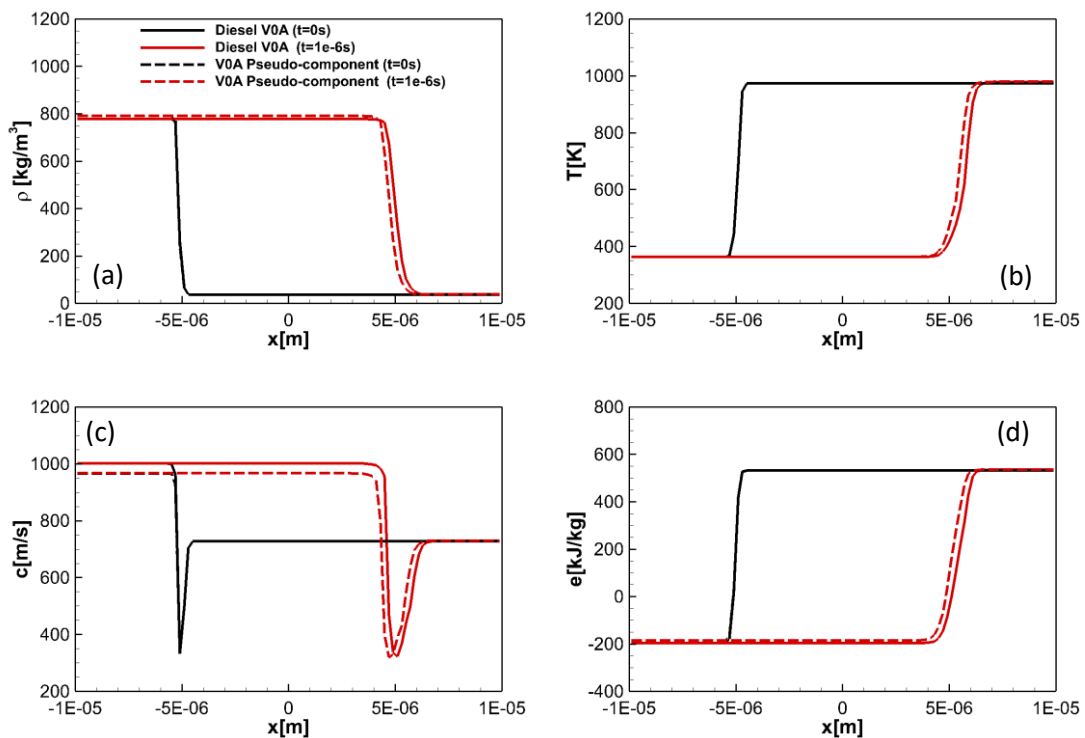
592 **Figure 12. Advection Test Case 2 (N_2- V0A/ pseudo-Diesel V0A), CFL = 0.5, u = 10 m/s,**
593 **100 cells. Results of (a) density, (b) temperature, (c) speed of sound and (d) internal energy**
594 **results at 10^{-6} s.**
595
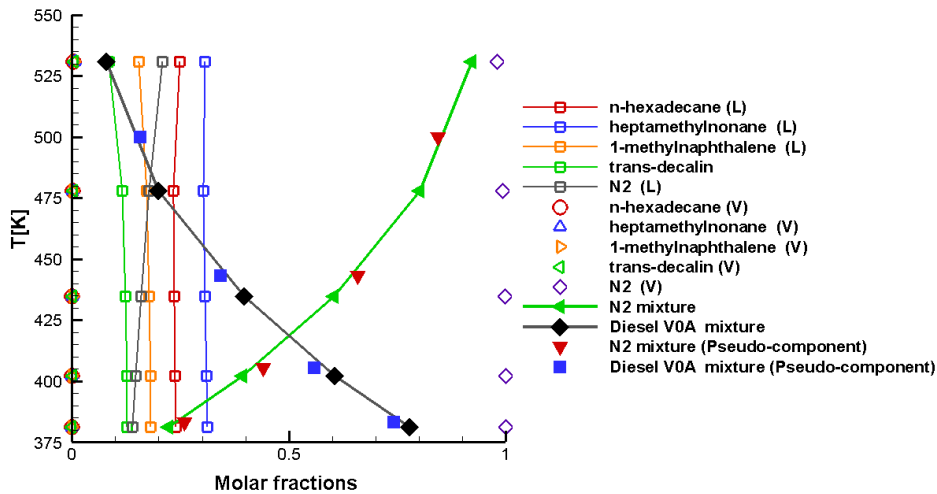
Figure 13. VLE Interface, Advection Test Case 2 (N_2- V0A/ pseudo-Diesel V0A), CFL= 0.5, u = 10 m/s, 100 cells. Results of VLE interface at 10^{-6}s.
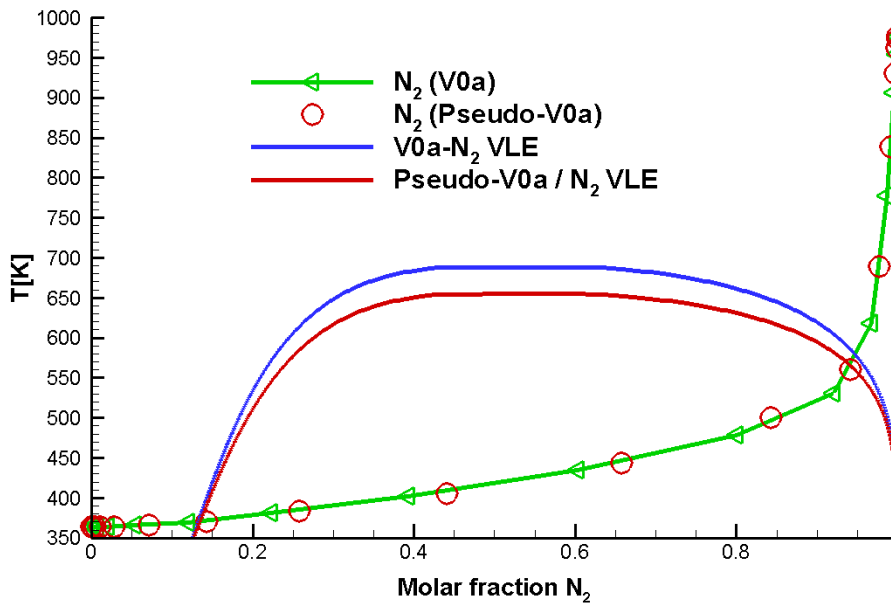
Figure 14. Advection Test Case 2 (N_2- V0A/ pseudo-Diesel V0A). Results of VLE interface at 10^{-6}s and phase boundaries from VLE at 11MPa.

3.c Two-dimensional cases

Planar two-dimensional injections of n-dodecane and a Diesel pseudo-component are presented to demonstrate the multidimensional capability of the numerical framework.

N-dodecane jet

A structured mesh is applied with a uniform cell distribution; the domain used is 12mm × 6mm; 1,216,800 cells are employed; the parabolic sub-step is included into these simulations without sub-grid scale modelling for turbulence or heat/species diffusion; the CFL number is set at 0.5; the fifth-order WENO discretization scheme presented in [18] is used; transmissive boundary conditions are applied at the top, bottom and right boundaries while a wall condition is employed at the left boundary; a flat velocity profile is imposed at the inlet; the velocity of

19

612   the jet is 600 m/s; the diameter of the exit nozzle is 0.1mm; the case is initialized using a
613   pressure in the chamber of 11 MPa; the temperature of the nitrogen is 973 K; and the
614   temperature of the injected fuel is 363K. The binary interaction parameter applied is k_{ij} =
615   0.1446. The loops where the hyperbolic fluxes, parabolic fluxes, update of conservative
616   variables and thermodynamic solver are solved (see Figure 2) were paralleled employing
617   OpenMP (24 physical cores where employed). Some instabilities were observed in the
618   initialization as [16] reported. To solve this problem, a ramp is used to accelerate the fuel to
619   600m/s. The jet is quickly heated-up from a compressed liquid state to gas and finally, to a
620   supercritical state describing an isobaric-adiabatic mixing line, see Figure 16. Figure 17 shows
621   how the Kelvin Helmholtz instability and ligament-shaped structures are developed in the shear
622   layer.
623
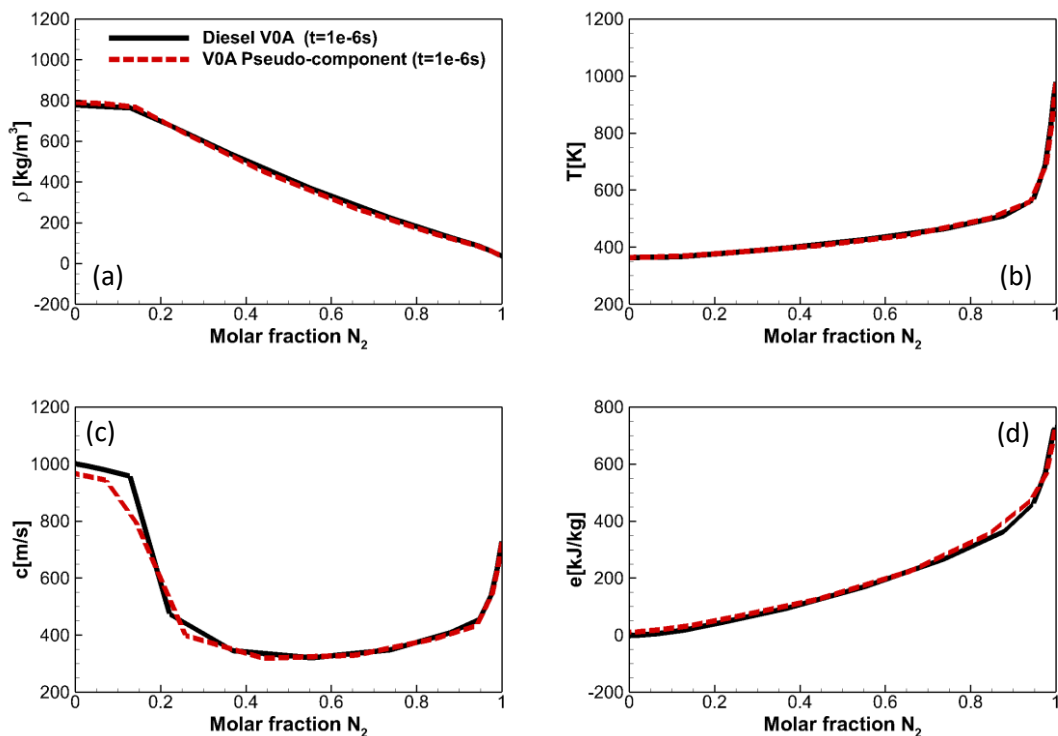
624   **Figure 15. Advection Test Case 2 (N_2- V0A/ pseudo-Diesel V0A), CFL = 0.5, u = 10 m/s,**
625   **100 cells. Results of (a) density, (b) temperature, (c) speed of sound and (d) internal energy**
626   **results at 10^{-6} s.**
627

628 **Diesel jet**
629   The initial conditions and set-up of the simulation is the same as the n-dodecane jet.
630   The binary interaction parameter applied is k_{ij} = 0.1446. Figure 18 shows the density,
631   temperature and pressure at 3.19×10^{-5} s. Spurious pressure oscillations are not present in the
632   pressure field despite the multicomponent nature of the simulations and large density gradients
633   solved. The simulation present supersonic, transonic and subsonic regions due to the low values
634   of the speed of sound present in the cells in a VLE state and the high jet velocity, see Figure
635   18. Such a variety of Mach numbers in a simulation can introduce important stability issues
636   However, stability problems were not observed. The computational time required to solve at
637   3.3×10^{-5}s was 91.7 hours. Most time is invested on solving the multidimensional Newton
638   method of the cells that are in a VLE state. At these conditions, the derivatives of the Jacobian
639   matrix are calculated numerically (Appendix 5). However, the developed methodology is fast

640 enough to perform simulations at affordable time scales. It should also be considered that the
641 results are equivalent to a multicomponent injection of a Diesel surrogate of 4 components that
642 vaporize when mixed with hot nitrogen.

643
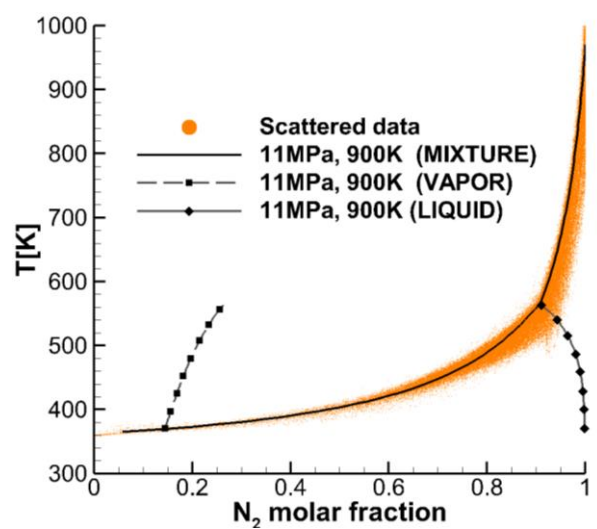
644
645 **Figure 16. Scattered data of composition and temperature of the planar n-dodecane jet,**
646 **dodecane-nitrogen phase boundary from VLE at 11MPa and isobaric-adiabatic mixing line.**

647
648
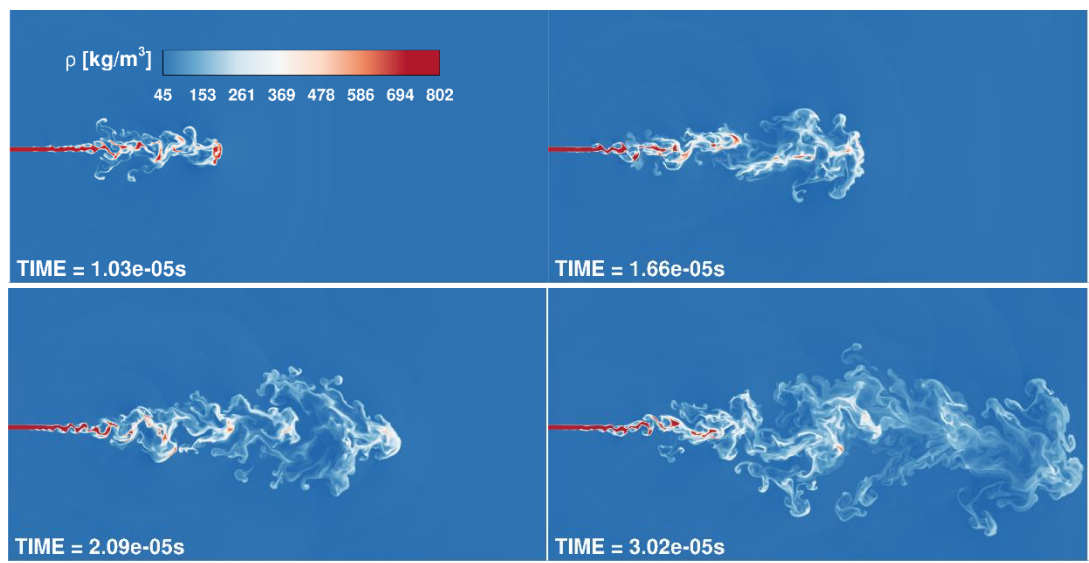
649
650
651 **Figure 17. Density results of n-dodecane planar jet.**

652 ## 4. Conclusions

653 This paper presents a numerical framework that combines PC-SAFT and VLE calculations in
654 a density-based, fully conservative solver of the Navier-Stokes and energy conservation
655 equations to simulate fuel-air mixing at high-pressure conditions. This molecular-based EoS
656 requires three empirically determined but well-known parameters to model the properties of a
657 specific component, and thus, there is no need for extensive model calibration, as is typically
658 the case when the NIST (REFPROP) library is utilised. PC-SAFT can flexibly handle the
659 thermodynamic properties of multi-component mixtures for which the NIST (REFPROP)
660 library supports only limited component combinations. Modelling multicomponent Diesel

surrogates, the PC-SAFT EoS shows the highest degree of agreement with experimental values in comparison with the results obtained using the model developed at NIST. Moreover, a purely predictive method that employs the PC-SAFT EoS for developing pseudo-components has been completed and validated to be used in CFD simulations. Complex hydrocarbon mixtures can be modelled as a single pseudo-component knowing its MW and HN/CN ratio. By employing pseudo-components, the simulation time is independent of the number of compounds present in the fuel and thus, allowing real fuel compositions to be utilised in CFD simulations. Advection test cases and shock tube problems were performed to validate the numerical framework using analytical and exact solutions. The two-dimensional simulations performed (subcritical injections of n-dodecane and Diesel into nitrogen) demonstrate the multidimensional, multispecies and multiphase capability of the algorithm and its high stability in simulations where all sonic regimes are present.
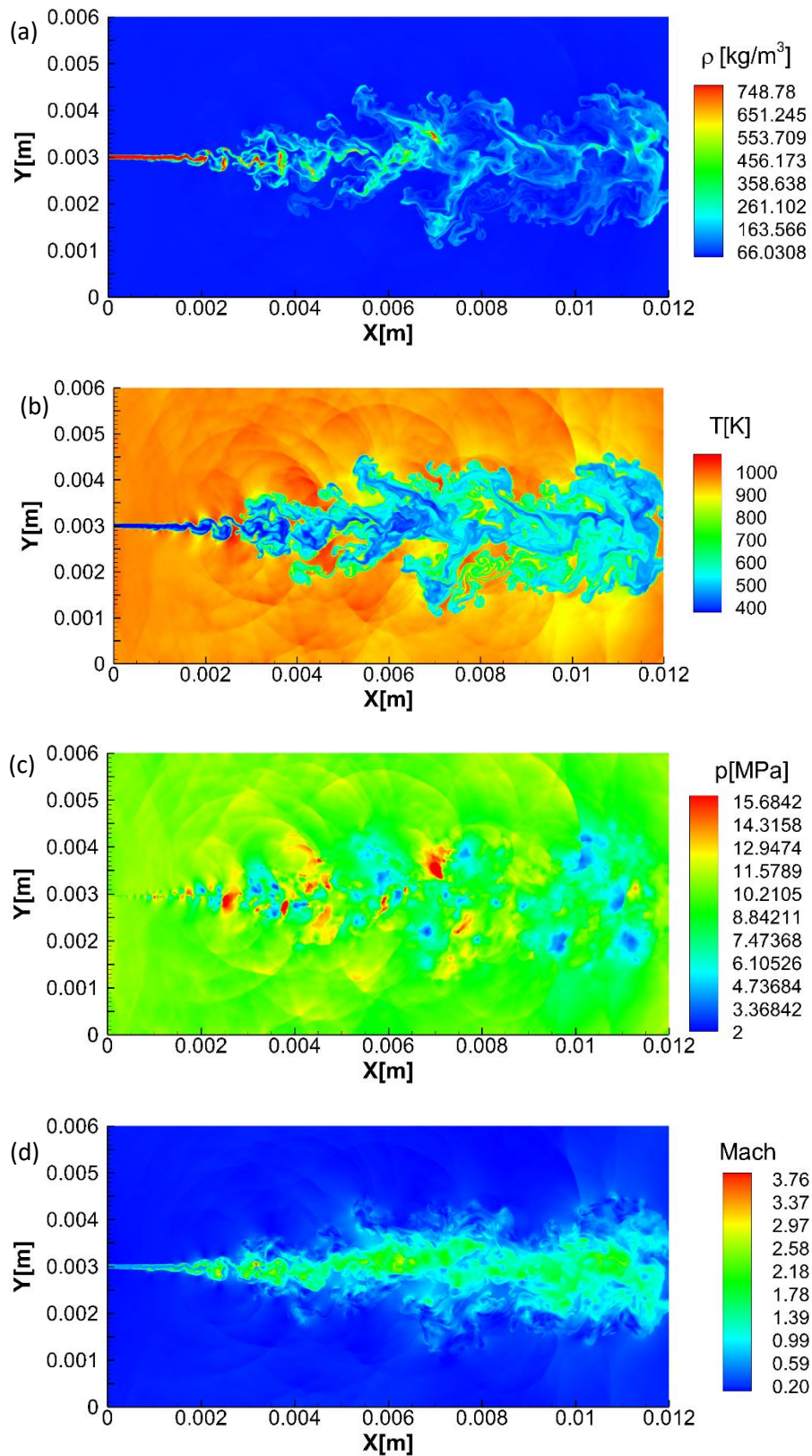
Figure 18. CFL = 0.5, 1,216,800 cells. Results of the simulation of the V0A Diesel pseudo-component jet at t = 3.19 x 10^{-5} s: (a) density, (b) temperature, (c) pressure and (d) Mach number.

Appendix 1 (CFD CODE)

The Navier-Stokes equations for a non-reacting multi-component mixture containing N species in a x-y 2D Cartesian system are given by:

$$\frac{\partial U}{\partial t} + \frac{\partial F}{\partial x} + \frac{\partial G}{\partial y} = \frac{\partial F_v}{\partial x} + \frac{\partial G_v}{\partial y} \tag{A.1}$$

The vectors of A.1 are:

$$\mathbf{U} = \begin{bmatrix} \rho Y_1 \\ \vdots \\ \rho Y_N \\ \rho u \\ \rho v \\ \rho E \end{bmatrix}, \mathbf{F} = \begin{bmatrix} \rho u Y_1 \\ \vdots \\ \rho u Y_N \\ \rho u^2 + p \\ \rho u v \\ (\rho E + p)u \end{bmatrix}, \mathbf{G} = \begin{bmatrix} \rho v Y_1 \\ \vdots \\ \rho v Y_N \\ \rho v u \\ \rho v^2 + p \\ (\rho E + p)v \end{bmatrix}, \mathbf{F_v} = \begin{bmatrix} J_{x,1} \\ \vdots \\ J_{x,N} \\ \sigma_{xx} \\ \sigma_{xy} \\ u\sigma_{xx} + v\sigma_{xy} - q_x \end{bmatrix}, \tag{A.2}$$

$$\mathbf{G_v} = \begin{bmatrix} J_{y,1} \\ \vdots \\ J_{y,N} \\ \sigma_{yx} \\ \sigma_{yy} \\ u\sigma_{yx} + v\sigma_{yy} - q_y \end{bmatrix}$$

where ρ is the fluid density, u and v are the velocity components, p is the pressure, E is the total energy, J_i is the mass diffusion flux of species i, σ is the deviatoric stress tensor and q is the diffusion heat flux vector.

Hyperbolic sub-step

The multicomponent HLLC (Harten-Lax-van Leer-Contact) solver is applied to solve the Riemann problem [36]. The fluxes are computed as:

$$\mathbf{F}^{HLLC} = \begin{cases} \mathbf{F_L} & \text{if} \quad 0 \leq S_L, \\ \mathbf{F_{*L}} = \mathbf{F_L} + S_L(\mathbf{U_{*L}} - \mathbf{U_L}) & \text{if} \quad S_L \leq 0 \leq S_*, \\ \mathbf{F_{*R}} = \mathbf{F_R} + S_R(\mathbf{U_{*R}} - \mathbf{U_R}) & \text{if} \quad S_* \leq 0 \leq S_{*R}, \\ \mathbf{F_R} & \text{if} \quad 0 \geq S_{*R}, \end{cases} \tag{A.3}$$

where U_* are the star states [36].

The speed in the middle wave is:

$$S_* = \frac{p_R - p_L + \rho_L u_L(S_L - u_L) - \rho_R u_R(S_R - u_R)}{\rho_L(S_L - u_L) - \rho_R(S_R - u_R)} \tag{A.4}$$

The left and right wave speeds are computed as:

$$S_L = min(u_L - a_L, u_R - a_R),$$
$$S_R = max(u_L + a_L, u_R + a_R) \tag{A.5}$$

717 The conservative variables, pressure and speed of sound values needed to solve the
718 Riemann problem are interpolated at the cell faces from cell centers using the fifth order
719 reconstruction scheme described in [18]. This technique decreases the computational time and
720 smooths-out the spurious pressure oscillations associated with fully conservative (FC) schemes
721 employed along with real-fluid EoS.

722

723 The temporal integration is carried out using a second-order Runge–Kutta (RK2)
724 scheme (A.6) applying the filter presented in [18].

725

726 $$\boldsymbol{U}^{(1)} = \boldsymbol{U}^n + \Delta t H_{xy}(\boldsymbol{U}^n),$$

727 $$\boldsymbol{U}^{n+1} = \frac{1}{2}\boldsymbol{U}^n + \frac{1}{2}\left[\boldsymbol{U}^{(1)} + \Delta t H_{xy}(\boldsymbol{U}^{(1)})\right] \tag{A.6}$$

728

729 **Parabolic sub-step**
730 The model developed by [37] is used to calculate the dynamic viscosity and the thermal
731 conductivity. The viscous stress tensor is calculated as:

732

733 $$\sigma_{xx} = 2\mu_v \frac{\partial u}{\partial x} - \frac{2}{3}\mu_v \left(\frac{\partial u}{\partial x} + \frac{\partial v}{\partial y}\right)$$

734 $$\sigma_{yy} = 2\mu_v \frac{\partial v}{\partial y} - \frac{2}{3}\mu_v \left(\frac{\partial u}{\partial x} + \frac{\partial v}{\partial y}\right)$$

735 $$\sigma_{xy} = \sigma_{yx} = \mu_v \left(\frac{\partial u}{\partial y} + \frac{\partial v}{\partial x}\right) \tag{A.7}$$

736

737 where μ_v is the viscosity.

738

739 The species mass diffusion flux of species i is calculated employing Fick's law:
740 $$J_i = \rho D_i \nabla Y_i - Y_i \sum_{j=1}^{Nc} \rho D_j \nabla Y_j \tag{A.8}$$
741 where
742 $$D_i = \frac{(1-z_i)}{\sum_{j\neq i}^{Nc} \frac{z_j}{D i_j}} \tag{A.9}$$

743 being D is the diffusion coefficient for the diffusion of the component i in the rest of the mixture
744 [52].

745

746 The heat flux vector is calculated as:
747 $$\boldsymbol{q} = -\lambda \nabla T - \sum_i^N h_i J_i \qquad \qquad ` \tag{A.10}$$
748 where λ is the thermal conductivity and $\mathbf{h}$ is the enthalpy.

749

750

Appendix 2 (Thermodynamic solver for stable mixtures)

The molecular density is computed using the density of the mixture. Once the molecular density is known a Newton method is employed to compute the temperature that is needed to calculate the value of all other thermodynamic variables. The temperature dependent function used in the iterative method is the internal energy. Initially a temperature value is assumed (for example the value of the temperature from the previous time RK sub-step or from the previous time step) to initialize the iteration process. In most cells, this value is close to the solution.

Algorithm 1 {

! Newton method (T)
DO
    1 CONTINUE
    If $\left[\left(\text{abs (e(CSV)-e(PC-SAFT))}\right)>0.001\right]$ then

Algorithm A {
Inputs: Temperature, density, molar composition
Outputs: Pressure, sonic fluid velocity, internal energy, enthalpy,
    partial derivative of the internal energy respects
    the temperature at constant density

Compute the new temperature value:

$$T^{n+1} = T^{n} + \left(\frac{\partial e}{\partial T}\right)_{\rho} T^{n}$$

    GO TO 1
    ELSE
        RETURN
    END IF
END DO
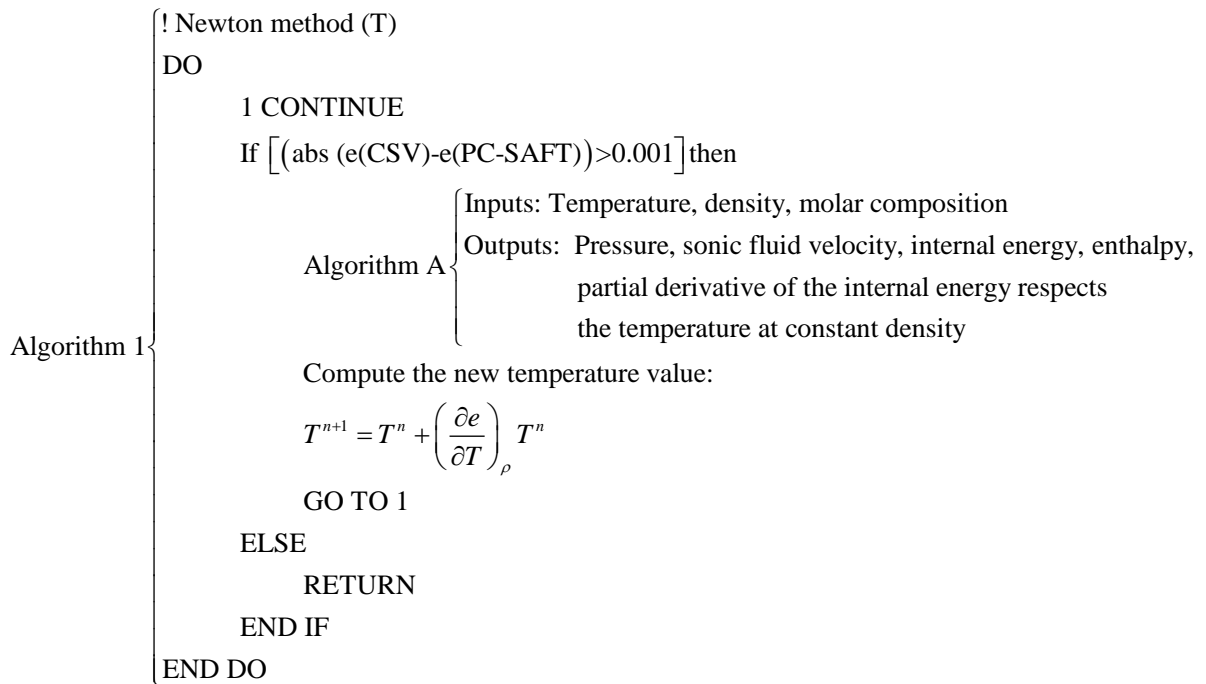
Figure A1. Schematic representation of the Algorithm 1

Appendix 3 (Algorithm A)

Inputs: Temperature, density, molar composition.

Output: Pressure, sonic fluid velocity, internal energy, enthalpy, partial derivative of the internal energy respects the temperature at constant density.

Algorithm A
1) Compute molecular density (A.11)
2) Compute segment diameter of each component (A.12)
3) Compute mean segment number (A.13)
4) Compute radial distribution function of the hard sphere fluid (A.14)
5) Compute hard sphere fluid contribution to the compressibility factor (A.16)
6) Compute hard chain contribution to the compressibility factor (A.17)
7) Compute dispersion contribution to the compressibility factor (A.19)
8) Compute total compressibility factor (A.30)
9) Compute pressure (A.31)
10) Compute the contribution of the hard-sphere system to the residual Helmholtz free energy temperature derivative (A.32)
11) Compute the hard-chain reference contribution to the residual Helmholtz free energy temperature derivative (A.35)
12) Compute the dispersion contribution to the residual Helmholtz free energy temperature derivative (A.37)
13) Compute the residual Helmholtz free energy temperature derivative (A.41)
14) Compute internal energy (A.43)
15) Compute enthalpy (A.45)
16) Compute heat capacities (A.46,A.47)
17) Compute sonic fluid velocity (A.50)
18) Compute the temperature derivative of the internal energy (A.58)
19) Compute the new temperature using the Newton-Raphson method

Figure A2. Schematic representation of the Algorithm A

Steps

1) **Compute molecular density**

$$\rho_m = \rho(kg/m^3)*10^{-30}*N_A/M_M*1000 \tag{A.11}$$

where N_A is the Avogadro number and M_M is the molecular weight of the mixture.

2) **Compute temperature-dependent segment diameter d of component i** [53]

$$d_i = \sigma_{di}\left[1 - 0.12\,exp\left(-3\frac{\varepsilon_i}{kT}\right)\right] \tag{A.12}$$

where k is the Boltzmann constant, T is the temperature, ε_i is the depth of pair potential of the component and σ_{di} is the segment diameter.

3) **Compute mean segment number** [53]

$$\bar{m} = \sum_i^{nc} x_i\,m_i \tag{A.13}$$

where m_i is the number of segments per chain of the component i and x_i is the mole fraction of component i.

4) **Compute radial distribution function of the hard-sphere fluid** [53]

27

$$g_{ij}^{hs} = \frac{1}{(1-\varsigma_3)} + \left(\frac{d_i d_j}{d_i+d_j}\right)\frac{3\varsigma_2}{(1-\varsigma_3)^2} + \left(\frac{d_i d_j}{d_i+d_j}\right)^2 \frac{3\varsigma_2^2}{(1-\varsigma_3)^3} \qquad (A.14)$$

where

$$\varsigma_n = \frac{\pi}{6}\rho_m \sum_i x_i m_i d_i^n \qquad\qquad n \in \{0,1,2,3\} \qquad (A.15)$$

5) Compute contribution of the hard sphere to the compressibility factor [53]

$$Z^{hs} = \frac{\varsigma_3}{(1-\varsigma_3)} + \frac{3\varsigma_1\varsigma_2}{\varsigma_0(1-\varsigma_3)^2} + \frac{3\varsigma_2^3 - \varsigma_3\varsigma_2^3}{\varsigma_0(1-\varsigma_3)^3} \qquad (A.16)$$

6) Compute hard-chain contribution to the compressibility factor [53]

$$Z^{hc} = \bar{m}Z^{hs} - \sum_i x_i (m_i - 1)(g_{ii}^{hs})^{-1}\rho_m \frac{\partial g_{ii}^{hs}}{\partial \rho_m} \qquad (A.17)$$

$$\rho \frac{\partial g_{ij}^{hs}}{\partial \rho} = \frac{\zeta_3}{(1-\zeta_3)^2} + \left(\frac{d_i d_j}{d_i+d_j}\right)\left(\frac{3\zeta_2}{(1-\zeta_3)^2} + \frac{6\zeta_2\zeta_3}{(1-\zeta_3)^3}\right) +$$

$$\left(\frac{d_i d_j}{d_i+d_j}\right)^2 \left(\frac{4\zeta_2^2}{(1-\zeta_3)^3} + \frac{6\zeta_2^2\zeta_3}{(1-\zeta_3)^4}\right) \qquad (A.18)$$

7) Compute dispersion contribution to the compressibility factor [53]

$$Z^{disp} = -2\pi\rho_m \frac{\partial(\eta I_1)}{\partial \eta}\overline{m^2\varepsilon\sigma_d^3} - \pi\rho_m\bar{m}\left[C_1\frac{\partial(\eta I_2)}{\partial \eta} + C_2\eta I_2\right]\overline{m^2\varepsilon^2\sigma_d^3} \qquad (A.19)$$

C_1 and C_2 are defined as:

$$C_1 = \left(1 + Z^{hc} + \rho\frac{\partial Z^{hc}}{\partial \rho}\right)^{-1} =$$

$$\left(1 + \overline{m}\frac{8\eta - 8\eta^2}{(1-\eta)^4} + (1-\overline{m})\frac{20\eta - 27\eta^2 + 12\eta^3 - 2\eta^4}{[(1-\eta)(2-\eta)]^2}\right)^{-1} \qquad (A.20)$$

$$C_2 = \frac{\partial C_1}{\partial \eta} = -C_1^2\left(\overline{m}\frac{-4\eta^2 + 20\eta + 8}{(1-\eta)^5} + (1-\overline{m})\frac{2\eta^3 + 12\eta^2 - 48\eta + 40}{[(1-\eta)(2-\eta)]^3}\right) \qquad (A.21)$$

The terms $\overline{m^2\varepsilon\sigma_d^3}$ and $\overline{m^2\varepsilon^2\sigma_d^3}$ are defined as:

$$\overline{m^2\varepsilon\sigma_d^3} = \sum_i^{nc}\sum_j^{nc} x_i x_j m_i m_j \left(\frac{\varepsilon_{ij}}{kT}\right)\sigma_{d,ij}^3 \qquad (A.22)$$

$$\overline{m^2\varepsilon^2\sigma_d^3} = \sum_i^{nc}\sum_j^{nc} x_i x_j m_i m_j \left(\frac{\varepsilon_{ij}}{kT}\right)^2\sigma_{d,ij}^3 \qquad (A.23)$$

The mixture parameters σ_{ij} and ε_{ij}, which are defined for every pair of unlike segments, are modelled using a Berthelot-Lorentz combining rule.

$$\sigma_{ij} = \frac{1}{2}(\sigma_i + \sigma_j) \qquad (A.24)$$

$$\varepsilon_{ij} = \sqrt{\varepsilon_i\varepsilon_j}(1 - k_{ij}) \qquad (A.25)$$

$\frac{\partial(\eta I_1)}{\partial \eta}$ and $\frac{\partial(\eta I_2)}{\partial \eta}$ are expressed as:

$$\frac{\partial(\eta I_1)}{\partial \eta} = \sum_{j=0}^6 a_j(\bar{m})(j+1)\eta^i \qquad (A.26)$$

$$\frac{\partial(\eta I_2)}{\partial \eta} = \sum_{j=0}^6 b_j(\bar{m})(j+1)\eta^i \qquad (A.27)$$

The coefficients a and b depend on the chain length:

$$a_i(\overline{m}) = a_{0i} + \frac{\overline{m}-1}{\overline{m}}a_{1i} + \frac{\overline{m}-1}{\overline{m}}\frac{\overline{m}-2}{\overline{m}}a_{2i} \qquad (A.28)$$

28

823      $b_i(\overline{m}) = b_{0i} + \frac{\overline{m}-1}{\overline{m}} b_{1i} + \frac{\overline{m}-1}{\overline{m}} \frac{\overline{m}-2}{\overline{m}} b_{2i}$ (A.29)

824      $a_{0i}, a_{1i}, a_{2i}, b_{0i}, b_{1i}, b_{2i}$ are constants [53].

825

826 **8) Compute compressibility factor [53]**

827      $Z = 1 + Z^{hc} + Z^{disp}$ (A.30)

828

829 **9) Compute pressure [53]**

830      $P = Z k_B T \rho_m (10^{10})^3$ (A.31)

831

832 **10) Compute temperature derivative of the Helmholtz free energy residual**
833   **contribution of the hard-sphere system [53]**

834

835
$$\left(\frac{\partial \tilde{a}^{hs}}{\partial T}\right)_{\rho,x_i} = \frac{1}{\varsigma_0}\left[\begin{array}{c} \frac{3(\varsigma_{1,T}\varsigma_2 + \varsigma_1\varsigma_{2,T})}{(1-\varsigma_3)} + \frac{3\varsigma_1\varsigma_2\varsigma_{3,T}}{(1-\varsigma_3)^2} + \frac{3\varsigma_2{}^2\varsigma_{2,T}}{\varsigma_3(1-\varsigma_3)^2} + \frac{\varsigma_2{}^3\varsigma_{3,T}(3\varsigma_3-1)}{\varsigma_3{}^2(1-\varsigma_3)^3} + \\ \left(\frac{3\varsigma_2{}^2\varsigma_{2,T}\varsigma_3 - 2\varsigma_2{}^3\varsigma_{3,T}}{\varsigma_3{}^3}\right)\ln(1-\varsigma_3) + \left(\varsigma_0 - \frac{\varsigma_2{}^3}{\varsigma_3{}^2}\right)\frac{\varsigma_{3,T}}{(1-\varsigma_3)} \end{array}\right]$$

836   (A.32)

837   with abbreviations for two temperature derivatives:

838      $\varsigma_{n,T} = \frac{\partial \varsigma_n}{\partial T} = \frac{\pi}{6}\rho \sum_i x_i m_i n d_{i,T}(d_i)^{n-1}$ $n \in \{0,1,2,3\}$ (A.33)

839      $d_{i,T} = \frac{\partial d_i}{\partial T} = \sigma_i\left(3\frac{\varepsilon_i}{kT^2}\right)\left[-0.12\exp\left(-3\frac{\varepsilon_i}{kT}\right)\right]$ (A.34)

840

841 **11) Compute temperature derivative of the Helmholtz free energy hard-chain**
842   **reference contribution [53]**

843

844      $\left(\frac{\partial \tilde{a}^{hc}}{\partial T}\right)_{\rho,x_i} = \bar{m}\left(\frac{\partial \tilde{a}^{hs}}{\partial T}\right)_{\rho,x_i} - \sum_i x_i (m_i - 1)(g_{ii}{}^{hs})^{-1}\left(\frac{\partial g_{ii}{}^{hs}}{\partial T}\right)_{\rho,x_i}$ (A.35)

845

846   The temperature derivative of the radial pair distribution function is:

847      $\frac{\partial g_{ii}{}^{hs}}{\partial T} = \frac{\varsigma_{3,T}}{(1-\varsigma_3)^2} + \left(\frac{1}{2}d_{i,T}\right)\frac{\varsigma_2}{(1-\varsigma_3)^2} + \left(\frac{1}{2}d_i\right)\left(\frac{3\varsigma_{2,T}}{(1-\varsigma_3)^2} + \frac{6\varsigma_2\varsigma_{3,T}}{(1-\varsigma_3)^3}\right) +$

848      $\left(\frac{1}{2}d_i d_{i,T}\right)\frac{2\varsigma_2{}^2}{(1-\varsigma_3)^3} + \left(\frac{1}{2}d_i\right)^2\left(\frac{4\varsigma_2\varsigma_{2,T}}{(1-\varsigma_3)^3} + \frac{6\varsigma_2{}^2\varsigma_{3,T}}{(1-\varsigma_3)^4}\right)$ (A.36)

849

850 **12) Compute temperature derivative of the Helmholtz free energy dispersive**
851   **attraction [53]**

852

853      $\left(\frac{\partial \tilde{a}^{disp}}{\partial T}\right)_{\rho,x_i} = -2\pi\rho\left(\frac{\partial I_1}{\partial T} - \frac{I_1}{\partial T}\right)\overline{m^2\varepsilon\sigma_d{}^3} - \pi\rho\overline{m}$

854      $\left[\frac{\partial C_1}{\partial T}I_2 + C_1\frac{\partial I_2}{\partial T} - 2C_1\frac{I_2}{T}\right]\overline{m^2\varepsilon^2\sigma_d{}^3}$ (A.37)

855   with

856      $\frac{\partial I_1}{\partial T} = \sum_{i=0}^6 a_i(\overline{m}) i \varsigma_{3,T} \eta^{i-1}$ (A.38)

857      $\frac{\partial I_2}{\partial T} = \sum_{i=0}^6 b_i(\overline{m}) i \varsigma_{3,T} \eta^{i-1}$ (A.39)

858
$$\frac{\partial C_1}{\partial T} = \varsigma_{3,T} C_2 \tag{A.40}$$

859

860 **13) Compute temperature derivative of the Helmholtz free energy** [53]

861

862
$$\left(\frac{\partial \tilde{a}^{res}}{\partial T}\right)_{\rho,x_i} = \left(\frac{\partial \tilde{a}^{hc}}{\partial T}\right)_{\rho,x_i} + \left(\frac{\partial \tilde{a}^{disp}}{\partial T}\right)_{\rho,x_i} \tag{A.41}$$

863

864 **14) Compute the internal energy** [54]

865 The internal energy is estimated as the sum of the ideal internal energy and the residual
866 internal energy [54].

867
$$\frac{e^{res}}{RT} = -T \left(\frac{\partial \tilde{a}^{res}}{\partial T}\right)_{\rho,x_i} \tag{A.42}$$

868
$$e = e^{res} + e^{id} \tag{A.43}$$

869

870 **15) Compute enthalpy** [53]**:**
871 It is computed as the sum of the ideal contribution (obtained by integrating the ideal
872 heat capacity at constant pressure with respect to the temperature) and the residual
873 enthalpy [53].

874
$$\frac{h^{res}}{RT} = -T \left(\frac{\partial \tilde{a}^{res}}{\partial T}\right)_{\rho,x_i} + (Z - 1) \tag{A.44}$$

875
$$h = h^{res} + h^{id} \tag{A.45}$$

876

877 **16) Heat capacities** [55]
878 Heat capacities are computed as the sum of the ideal contribution [56] and the
879 correction terms calculated with the PC-SAFT EoS [54]. where C_p and C_v are the heat
880 capacities at constant pressure and volume respectively.

881
$$C_v = C_{v,id} + C_{v,res} \tag{A.46}$$

882
$$C_p = C_{p,id} + C_{p,res} \tag{A.47}$$

883
$$C_v^{res} = -RT \left[2\left(\frac{\partial \tilde{a}^{res}}{\partial T}\right)_{\rho,x_i} + T\left(\frac{\partial^2 \tilde{a}^{res}}{\partial T^2}\right)_{\rho,x_i} \right] \tag{A.48}$$

884
$$C_p^{res} = C_v^{res} + R \frac{\left[\rho_m T\left(\frac{\partial^2 \tilde{a}^{res}}{\partial \rho_m \partial T}\right)_{x_i} + \rho_m\left(\frac{\partial \tilde{a}^{res}}{\partial \rho_m}\right)_{T,x_i} + 1\right]^2}{\left[\rho_m^2\left(\frac{\partial^2 \tilde{a}^{res}}{\partial \rho_m^2}\right)_{T,x_i} + 2\rho_m\left(\frac{\partial \tilde{a}^{res}}{\partial \rho_m}\right)_{T,x_i} + 1\right]} \tag{A.49}$$

885

886 **17) Speed of sound** [55]
887 The speed of sound is computed as:

888
$$c = \sqrt{\frac{C_p}{C_v}\left(\frac{\partial P}{\partial \rho_m}\right)_T} \tag{A.50}$$

889

890 The derivatives needed to compute the speed of sound are:

891
$$\left(\frac{\partial P}{\partial \rho_m}\right)_{T,x_i} = \left(\frac{\partial P}{\partial \eta}\right)_{T,x_i}\left(\frac{\partial \eta}{\partial \rho_m}\right)_{T,x_i} \tag{A.51}$$

892

$$\left(\frac{\partial \eta}{\partial \rho_m}\right)_{T,x_i} = \frac{\pi}{6}\left(\sum_i x_i m_i d_i^3\right) \tag{A.52}$$

893

$$\left(\frac{\partial P}{\partial \eta}\right)_{T,x_i} = k_B T (10^{10})^3 \left[\rho_m \left(\frac{\partial Z}{\partial \eta}\right)_{T,x_i} + Z \left(\frac{\partial \rho_m}{\partial \eta}\right)_{T,x_i}\right] \tag{A.53}$$

894

$$\left(\frac{\partial \rho_m}{\partial \eta}\right)_{T,x_i} = \frac{6}{\pi}\left(\sum_i x_i m_i d_i^3\right)^{-1} \tag{A.54}$$

895

$$\left(\frac{\partial Z}{\partial \eta}\right)_{T,x_i} \text{ can be found in [57].} \tag{A.55}$$

896

897 **18) Compute derivative internal energy respect temperature at constant density** [55]

898

899

$$\left(\frac{\partial e^{res}}{\partial T}\right)_{\rho,x_i} = -RT\left[2\left(\frac{\partial \tilde{a}^{res}}{\partial T}\right)_{\rho,x_i} + \left(\frac{\partial^2 \tilde{a}^{res}}{\partial T^2}\right)_{\rho,x_i} * T\right] \tag{A.56}$$

900

$$\frac{de^{id}}{dT} = C_v^{id} \tag{A.57}$$

901

902

$$\left(\frac{\partial e}{\partial T}\right)_{\rho,x_i} = \left(\frac{\partial e^{res}}{\partial T}\right)_{\rho,x_i} + \frac{de^{id}}{dT} \tag{A.58}$$

903

904 **19) Compute the new temperature using the Newton method**

905

906

907

908

909

910

911

912

913

914

915

916

917

918

919

920

921

922

923

924

925

Appendix 4 (Thermodynamic solver for mixtures at an unknown state)

The pressure and the temperature are iterated employing a multidimensional Newton method until the density and the internal energy obtained in the PC-SAFT are the ones obtained from the conservative variables. The initial values of the pressure and the temperature are the ones already stored in the cell that is being solved.

```
!Multidimensional Newton (P,T)
DO
    2 CONTINUE
    If [(abs (e(CSV)-e(VLE))>0.001].AND.[(abs (ρ(CSV)-ρ(VLE))>0.001] then
        Perform Stabiblity Analisys (SSI)
        IF(STABLE = .TRUE.)
```

Algorithm B

Inputs: Temperature, pressure, molar composition
Outputs: Density, sonic fluid velocity, internal energy, enthalpy, partial derivative of the internal energy respects the temperature at constant density

$$\left(\frac{\partial \rho}{\partial p}\right)_t, \left(\frac{\partial \rho}{\partial t}\right)_p, \left(\frac{\partial e}{\partial p}\right)_t, \left(\frac{\partial e}{\partial t}\right)_p$$

```
        ELSE
            Call TPn algorithm
        END IF
    Compute the new temperature and pressure values:
```

Algorithm 2

$$\begin{bmatrix} p \\ t \end{bmatrix}_{n+1} = \begin{bmatrix} p \\ t \end{bmatrix}_n - \left[\mathbf{J^{-1}}(p,t)_n\right]\begin{bmatrix} \rho(p,t)_n \\ e(p,t)_n \end{bmatrix}$$

$$\mathbf{J} = \begin{bmatrix} \left(\frac{\partial \rho}{\partial p}\right)_t & \left(\frac{\partial \rho}{\partial t}\right)_p \\ \left(\frac{\partial e}{\partial p}\right)_t & \left(\frac{\partial e}{\partial t}\right)_p \end{bmatrix}$$

```
    GO TO 2
    ELSE
    RETURN
    END IF
END DO
```

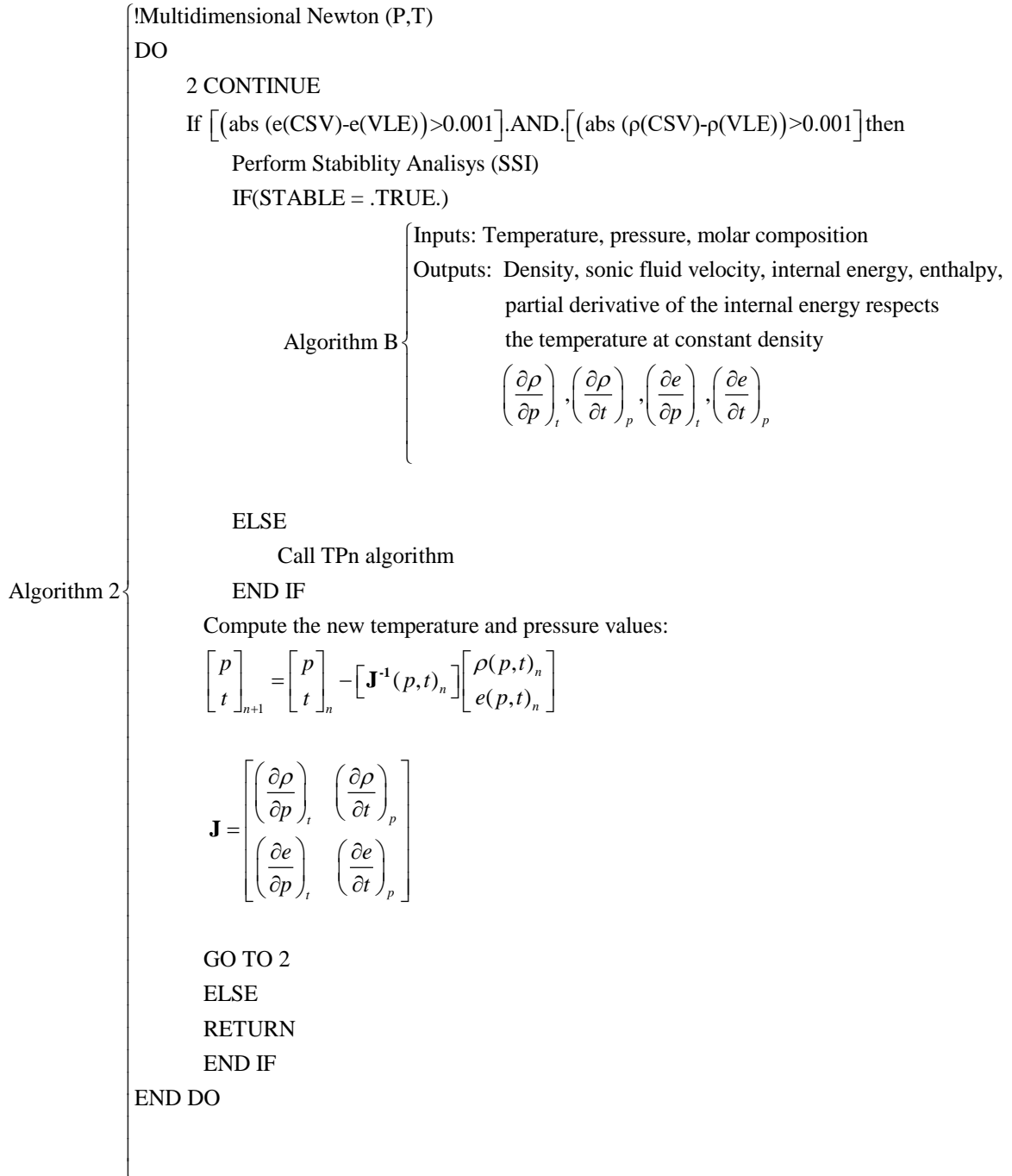**Figure A3. Schematic representation of the Algorithm 2**

Appendix 5 (Algorithm B)

Inputs: Temperature, pressure, molar composition.

Output: Density, speed of sound, internal energy, enthalpy, fugacities, partial derivative of the internal energy respect the temperature at constant pressure, partial derivative of the internal energy respect the pressure at constant temperature, partial derivative of the density respects the temperature at constant pressure and partial derivative of the density respect the temperature at constant pressure.

This algorithm is applied when the pressure and the temperature are iterated employing a multidimensional Newton method until the density and the internal energy computed are the ones obtained from the conservative variables.

$$\begin{bmatrix} p \\ t \end{bmatrix}_{n+1} = \begin{bmatrix} p \\ t \end{bmatrix}_n - [J^{-1}(p,t)_n] \begin{bmatrix} \rho(p,t)_n \\ e(p,t)_n \end{bmatrix} \tag{A.59}$$

where

$$J = \begin{bmatrix} \left(\frac{\partial \rho}{\partial p}\right)_t & \left(\frac{\partial \rho}{\partial t}\right)_p \\ \left(\frac{\partial e}{\partial p}\right)_t & \left(\frac{\partial e}{\partial t}\right)_p \end{bmatrix} \tag{A.60}$$

The independent variables of the PC-SAFT are the temperature and the density. Thus, it is necessary to perform the following transformations to obtain the partial derivatives needed for the multidimensional Newton method.

$$\left(\frac{\partial \rho}{\partial p}\right)_T = \left(\frac{\partial p}{\partial \rho}\right)_T^{-1} \qquad \text{Reciprocity} \tag{A.61}$$

$$\left(\frac{\partial \rho}{\partial t}\right)_p = -\left(\frac{\partial p}{\partial t}\right)_\rho \left(\frac{\partial p}{\partial \rho}\right)_T^{-1} \qquad \text{Chain rule} \tag{A.62}$$

$$\left(\frac{\partial e}{\partial p}\right)_T = \left(\frac{\partial e}{\partial \rho}\right)_T \left(\frac{\partial p}{\partial \rho}\right)_T^{-1} \qquad \text{Chain rule} \tag{A.63}$$

$$\left(\frac{\partial e}{\partial t}\right)_p = \left(\frac{\partial e}{\partial t}\right)_\rho - \left(\frac{\partial e}{\partial \rho}\right)_T \left(\frac{\partial \rho}{\partial t}\right)_\rho \left(\frac{\partial p}{\partial \rho}\right)_T^{-1} \qquad \text{Triple product rule} \tag{A.64}$$

The partial derivatives needed then are:

$$\left(\frac{\partial p}{\partial t}\right)_\rho, \left(\frac{\partial p}{\partial \rho}\right)_T, \left(\frac{\partial e}{\partial \rho}\right)_T, \left(\frac{\partial e}{\partial t}\right)_\rho$$

Steps
1) **Compute temperature-dependent segment diameter d of component i (A.12)**
2) **Compute mean segment number (A.13)**
3) **Compute radial distribution function of the hard-sphere fluid (A.14)**
4) **Reduce density iterative method**
   a. $\eta_{INIT} = 0.45$
   b. **Compute contribution of the hard sphere to the compressibility factor (A.16)**
   c. **Compute hard-chain contribution to the compressibility factor (A.17)**

Algorithm B {

1) Compute segment diameter of each component (A.12)

2) Compute mean segment number (A.13)

3) Compute radial distribution function of the hard sphere fluid (A.14)

4) Reduce density iterative method {

$\eta_{INIT} = 0.45$

DO

If $\left[\left(\text{abs}\ (p^{calc}\text{-}p^{sys})\right) > 0.001\right]$ *then*

    Compute hard sphere fluid contribution to the compressibility factor (A.16)

    Compute hard chain contribution to the compressibility factor (A.17)

    Compute dispersion contribution to the compressibility factor (A.19)

    Compute total compressibility factor (A.30)

    Compute pressure (A.31)

    Derivative of pressure respect resuce density

    Compute new pressure using Newton method

END IF

END DO

}

5) Compute the contribution of the hasd-sphere system to the residual Helmholtz free energy temperature derivative (A.32)

6) Compute the hard-chain reference contribution to the residual Helmholtz free energy temperature derivative (A.35)

7) Compute the dispersion contribution to the residual Helmholtz free energy temperature derivative (A.37)

8) Compute the residual Helmholtz free energy temperature derivative (A.41)

9) Compute internal energy (A.43)

10) Compute enthalpy (A.45)

11) Compute heat capacities (A.46,A.47)

12) Compute speed of sound (A.50)

13) Compute the derivatives of the Helmholtz free energy residual contribution of the hard-sphere system respect the molar fraction of the components $(A.66)$

14) Compute the derivative of the hard-chain reference contribution to the residual Helmholtz free energy respect the molar fraction of the components $(A.68)$

Algorithm B {

15) Compute derivative of the dispersion contribution to the residual Helmholtz free energy respect the molar fraction of the components $(A.70)$

16) Compute the chemical potential $(A.78)$

17) Compute the fugacity coefficient $(A.79)$

18) Compute the partial derivative of the pressure respect the density at constant temperature $(A.80)$

19) Compute the partial derivative of the pressure respect the temperature at constant density $(A.81)$

20) Compute the partial derivative of the internal energy respect the temperature at contant density $(A.58)$

21) Compute the partial derivative of the internal energy respect the density at constant temperature $(A.84)$

22) Compute the partial derivative of the density respect the pressure at constant temperature $(A.61)$

23) Compute the partial derivative of the density respect the temperature at constant pressure $(A.62)$

24) Compute the partial derivative of the internal energy respect the pressure at constant temperature $(A.63)$

25) Compute the partial derivative of the internal energy respect the temperature at constant pressure $(A.64)$

}

976

977

978   **Figure A4 Schematic representation of the Algorithm B**

979

980

981   **d. Compute dispersion contribution to the compressibility factor (A.19)**

982   **e. Compute compressibility factor (A.30)**

983   **f. Compute pressure (A.31)**

984   **g. Derivative of pressure respect reduce density**

985

986
$$\left(\frac{\partial P}{\partial \eta}\right) = \left[\rho_m \left(\frac{\partial Z}{\partial \eta}\right) + Z \left(\frac{\partial \rho_m}{\partial \eta}\right)\right] (10^{10})^3 Z k_B T \tag{A.65}$$

987

988   **h. Compute the new pressure using the Newton method**

989 **5) Compute temperature derivative of the Helmholtz free energy residual**
990   **contribution of the hard-sphere system (A.32)**

991 **6) Compute temperature derivative of the hard-chain reference contribution to the**
992   **residual Helmholtz free energy (A.35)**

993 **7) Compute temperature derivative of the dispersion contribution to the residual**
994   **Helmholtz free energy (A.37)**

995 **8) Compute temperature derivative of the Helmholtz free energy (A.41)**

996 **9) Compute the internal energy (A.43)**

997 **10) Compute enthalpy (A.45)**

998 **11) Compute heat capacities (A.46-47)**

999 **12) Compute speed of sound (A.50)**

1000 **13) Compute the derivatives of the Helmholtz free energy residual contribution of the**
1001   **hard-sphere system respect the molar fraction of the components.**

1002

1003
$$\left(\frac{\partial \tilde{a}^{hs}}{\partial x_k}\right)_{T,\rho,x_{j\neq k}} = -\frac{\zeta_{0,xk}}{\zeta_0}\tilde{a}^{hs} + \frac{1}{\zeta_0}\left[\frac{3(\zeta_{1,xk}\zeta_2 + \zeta_1\zeta_{2,xk})}{(1-\zeta_3)} + \frac{3\zeta_1\zeta_2\zeta_{3,xk}}{(1-\zeta_3)^2} + \frac{3\zeta_2^2\zeta_{2,xk}}{\zeta_3(1-\zeta_3)^2} + \right.$$

1004
$$\left. \frac{\zeta_2^3\zeta_{3,xk}(3\zeta_3-1)}{\zeta_3^2(1-\zeta_3)^3} + \left(\frac{3\zeta_2^2\zeta_{2,xk}\zeta_3 - 2\zeta_2^3\zeta_{3,xk}}{\zeta_3^3} - \zeta_{0,xk}\right)\ln(1-\zeta_3) + \left(\zeta_0 - \frac{\zeta_2^3}{\zeta_3^2}\right)\frac{\zeta_{3,xk}}{(1-\zeta_3)}\right] \tag{A.66}$$

1005

1006 where

1007
$$\zeta_{n,xk} = \left(\frac{\partial \zeta_n}{\partial x_k}\right)_{T,\rho,x_{j\neq k}} = \frac{\pi}{6}\rho m_k (d_k)^n \tag{A.67}$$

1008

1009 **14) Compute the derivative of the hard-chain reference contribution to the residual**
1010   **Helmholtz free energy respect the molar fraction of the components.**

1011
$$\left(\frac{\partial \tilde{a}^{hc}}{\partial x_k}\right)_{T,\rho,x_{j\neq k}}$$

1012
$$= m_k \tilde{a}^{hs} + \bar{m}\left(\frac{\partial \tilde{a}^{hs}}{\partial x_k}\right)_{T,\rho,x_{j\neq k}} - \sum_i x_i (m_i - 1)(g_{ii}^{hs})^{-1}\left(\frac{\partial g_{ii}^{hs}}{\partial x_k}\right)_{T,\rho,x_{j\neq k}}$$

1013
$$\tag{A.68}$$

1014 where

1015

1017
$$\left(\frac{\partial g_{ij}^{hs}}{\partial x_k}\right)_{T,\rho,x_{j\neq k}} = \frac{\zeta_{3,xk}}{(1-\zeta_3)^2} + \left(\frac{d_i d_j}{d_i + d_j}\right)\left(\frac{3\zeta_{2,xk}}{(1-\zeta_3)^2} + \frac{6\zeta_2\zeta_{3,xk}}{(1-\zeta_3)^3}\right)$$

1018
$$+ \left(\frac{d_i d_j}{d_i + d_j}\right)^2 \left(\frac{4\zeta_2\zeta_{2,xk}}{(1-\zeta_3)^3} + \frac{6\zeta_2^2\zeta_{3,xk}}{(1-\zeta_3)^4}\right) \tag{A.69}$$

1016

15) Compute derivative of the dispersion contribution to the residual Helmholtz free energy respect the molar fraction of the components.

$$\left(\frac{\partial \tilde{a}^{disp}}{\partial x_k}\right)_{T,\rho,x_{j\neq k}} = -2\pi\rho\left[I_{1,xk}\overline{m^2\varepsilon\sigma^3} + I_1\overline{(m^2\varepsilon\sigma^3)}_{xk}\right] -$$

$$\pi\rho\left\{\left[m_k C_1 I_2 + \overline{m}C_{1,xk}I_2 + \overline{m}C_1 I_{2,xk}\right]\overline{m^2\varepsilon\sigma^3} + \right.$$

$$\left.\overline{m}C_1 I_2 \overline{(m^2\varepsilon\sigma^3)}_{xk}\right\} \tag{A.70}$$

where

$$\overline{(m^2\varepsilon\sigma^3)}_{xk} = 2m_k\sum_j x_j m_j\left(\frac{\varepsilon_{kj}}{kT}\right)\sigma_{kj}^3 \tag{A.71}$$

$$\overline{(m^2\varepsilon^2\sigma^3)}_{xk} = 2m_k\sum_j x_j m_j\left(\frac{\varepsilon_{kj}}{kT}\right)^2\sigma_{kj}^3 \tag{A.72}$$

$$C_{1,xk} = C_2\zeta_{3,xk} - C_1^2\left[m_k\frac{8\eta-2\eta^2}{(1-\eta)^4} - m_k\frac{20\eta-27\eta^2+12\eta^3-2\eta^4}{[(1-\eta)(2-\eta)]^2}\right] \tag{A.73}$$

$$I_{1,xk} = \sum_{i=0}^{6}\left[a_i(\bar{m})i\zeta_{3,xk}\eta^{i-1} + a_{i,xk}\eta^i\right] \tag{A.74}$$

$$I_{2,xk} = \sum_{i=0}^{6}\left[b_i(\bar{m})i\zeta_{3,xk}\eta^{i-1} + b_{i,xk}\eta^i\right] \tag{A.75}$$

$$a_{i,xk} = \frac{m_k}{\overline{m}^2}a_{1i} + \frac{m_k}{\overline{m}^2}\left(3 - \frac{4}{\overline{m}}\right)a_{2i} \tag{A.76}$$

$$b_{i,xk} = \frac{m_k}{\overline{m}^2}b_{1i} + \frac{m_k}{\overline{m}^2}\left(3 - \frac{4}{\overline{m}}\right)b_{2i} \tag{A.77}$$

16) Compute the chemical potential.

$$\frac{\mu_k^{res(T,v)}}{kT} = \tilde{a}^{res} + (Z - 1) + \left(\frac{\partial\tilde{a}^{res}}{\partial x_k}\right)_{T,v,x_{i\neq j}} - \sum_{j=1}^{N}\left[x_j\left(\frac{\partial\tilde{a}^{res}}{\partial x_j}\right)_{T,v,x_{i\neq j}}\right] \tag{A.78}$$

17) Compute the fugacity coefficient.

$$ln\varphi_k = \frac{\mu_k^{res(T,v)}}{kT} - ln\,Z \tag{A.79}$$

18) Compute the partial derivative of the pressure respect the density at constant temperature.

$$\left(\frac{\partial P}{\partial \rho_m}\right)_T = k_B T(10^{10})^3\left[\left(\frac{\partial Z}{\partial \rho_m}\right)_t\rho_m + Z\right] \tag{A.80}$$

19) Compute the partial derivative of the pressure respect the temperature at constant density.

$$\left(\frac{\partial P}{\partial T}\right)_\rho = k_B(10^{10})^3\rho_m\left[\left(\frac{\partial Z}{\partial T}\right)_\rho T + Z\right] \tag{A.81}$$

20) Compute the partial derivative of the inernal energy respect the temperature at constant density (A.58)

21) Compute the partial derivative of the internal energy respect the density at constant temperature.

$$\left(\frac{\partial e^{res}}{\partial \rho_m}\right)_T = -RT^2\left(\frac{\partial\tilde{a}^{res}}{\partial T\partial \rho_m}\right)_T \tag{A.82}$$

1057 $$\frac{de^{id}}{d\rho_m} = 0.0 \tag{A.83}$$

1058

1059 $$\left(\frac{\partial e}{\partial T}\right)_{\rho,x_i} = \left(\frac{\partial e^{res}}{\partial T}\right)_{\rho,x_i} \tag{A.84}$$

1060

1061 **22) Compute the partial derivative of the density respect the pressure at constant**
1062   **tmeperature (A.61)**
1063 **23) Compute the partial derivative of the density respect the temperature at constant**
1064   **pressure (A.62)**
1065 **24) Compute the partial derivative of the internal energy respect the pressure at**
1066   **constant temperature (A.63)**
1067 **25) Compute the partial derivative of the internal energy respect the temperature at**
1068   **constant pressure (A.64)**

1069
1070
1071
1072
1073
1074
1075
1076
1077
1078
1079
1080
1081
1082
1083
1084
1085
1086
1087
1088
1089
1090
1091
1092
1093
1094
1095
1096
1097

Appendix 6 (Stability)

Input: Temperature, pressure and molar composition of the mixture.

Output: To know if the mixture is stable or not (one or two phases).

The Successive Substitution Iteration (SSI) algorithm ([16], [46]) (without the Newton method) has been employed.

$Stability$
$\begin{cases}\end{cases}$

1) IF (T > T_c FUEL) THEN

    STABLE=1

    RETURN

  END IF

2) IF$\left[(X_{N2} > C).AND.(X_{N2} < D)\right]$ THEN

    STABLE=0

    RETURN

  END IF

3) Call Algorithm B (obtain fugacity values)

    Inputs: Temperature, pressure, molar composition of the mixture

4) Calculate $d_i(z)$ (A.75)

5) Wilcom´s correlation is used to initialize the K-values (A.76)

6) Calculaten Y_init (A.77-A.78)

7) DO k=1,ntrial   ! SSI ALGORITHM

    Y_i = Y_init(k,i)

    DO j=1,nmax

      IF ($\|dY\| > \varepsilon_{SSI}$) THEN

          $y\_trial_i = Y_i/sum(Y)$

          Call Algorithm B

          $\begin{cases} \text{Inputs: Temperature, pressure, molar composition y\_trial} \\ \text{Obtain fugacity values } (\ln\varphi_i) \end{cases}$

          $Yn(i) = \exp\left[d_i(z) - \ln\varphi_i\right]$

          $dY_i = Yn_i - Y_i$

          $Y_i = Yn_i$

      ELSE

          TPD*(k) = 1. - sum(Y)

          GO TO 1

      END IF

    END DO

1 CONTINUE

IF (min(TPD*(k))< -10^{-8}

    STABLE = FALSE

ELSE

    STABLE =TRUE

END IF

END DO

Figure A5 Schematic representation of the stability algorithm

1107 **Steps**

1108   1) **The mixture is stable if the temperature is higher than T$_c$ Fuel (STABLE = 1)**
1109   Any mixture with a temperature higher than the fuel critical temperature will not be in
1110   a VLE state (STABLE = 1). This kind of filters are applied to reduce the computational
1111   time.

1113   2) **The mixture is unstable if the nitrogen molar fraction is bigger than C and lower**
1114   **than D (STABLE = 0)**
1115   The coefficients B and C are case dependent. For example, by performing an injection
1116   of n-dodecane at 363K in a combustion chamber at 900K, the nitrogen mole fraction at
1117   which the fuel starts vaporizing depends on the pressure in the combustion chamber.
1118   Considering Diesel engines at high-load operation conditions (11MPa) it would be safe
1119   to consider that any mixture with a nitrogen molar fraction bigger than 0.35 and lower
1120   than 0.7 will be in a VLE state, see Figure 4.

1122   3) **Call Algorithm B to obtain fugacity coefficient values $ln\varphi_i(z_i)$**
1123   **Inputs**: Temperature, pressure, molar composition of the mixture

1125   4) **Calculate $d_i(z)$**
1126 $$d_i(z) = ln\varphi_i(z_i) + lnz_i \tag{A.85}$$

1128   5) **The Wilcom´s correlation is used to initialize the K-values**
1129 $$K_i = \frac{p_{ci}}{p} exp\left[5.37(1.0 + w_i)\left(1.0 - \frac{T_{ci}}{T}\right)\right] \tag{A.86}$$
1130   being
1131 $$K_i = \frac{x_i}{y_i}$$
1132   where p_{ci} is the critical pressure of the component i, T_{ci} is the critical temperature of
1133   the component i, w_i is the acentric factor of the component i.

1135   6) **Calculate trial phases Y (two trials)**

1137   For the trial 1:
1138 $$Y(1, comp) = \begin{cases} \frac{z_i}{K_i} \text{ (Liquid phase)} \\ z_i K_I \text{ (Vapor phase)} \end{cases} \tag{A.87}$$

1140   For the trial 2:
1141 $$Y(2, comp) = \begin{cases} \frac{z_i}{K_i 3} \quad \text{(Liquid phase)} \\ \frac{z_i K_I}{3} \quad \text{(Vapor phase)} \end{cases} \tag{A.88}$$
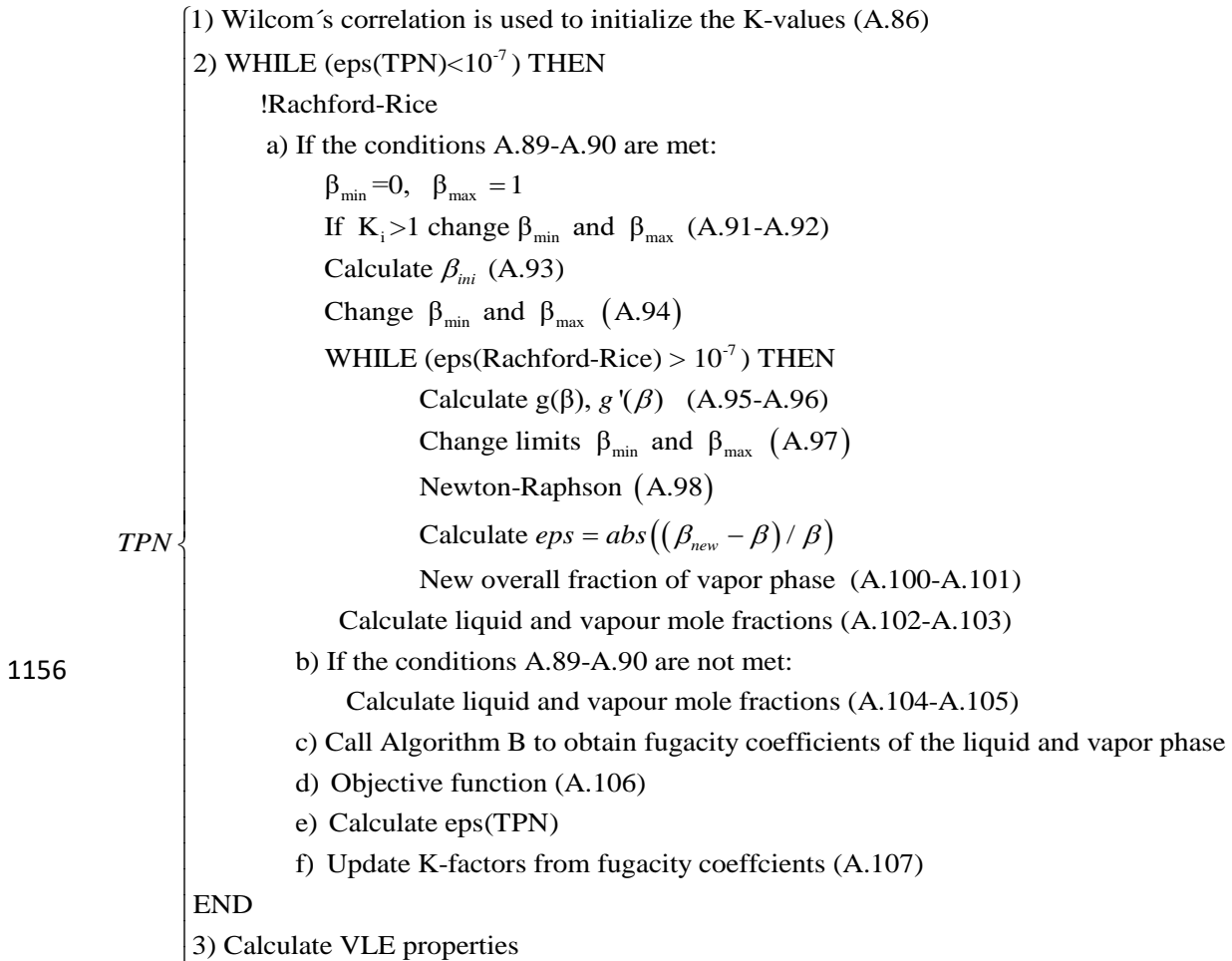
1143   7) **SSI-Algorithm described in Figure A5**.

Appendix 7 (TPn Algorithm)

Input: Temperature, pressure and molar composition of the mixture.

Output: Density of the mixture, internal energy of the mixture, speed of sound of the mixture and enthalpy of the mixture.

This algorithm is employed to to perform equilibrium calculations at specified temperature, pressure and overall composition. A successive substitution method is employed [16], [44].

TPN {
1) Wilcom´s correlation is used to initialize the K-values (A.86)

2) WHILE (eps(TPN)<10^{-7}) THEN

    !Rachford-Rice

    a) If the conditions A.89-A.90 are met:

        $\beta_{min}=0$, $\beta_{max}=1$

        If $K_i>1$ change β_{min} and β_{max} (A.91-A.92)

        Calculate β_{ini} (A.93)

        Change β_{min} and β_{max} (A.94)

        WHILE (eps(Rachford-Rice) > 10^{-7}) THEN

            Calculate g(β), $g'(\beta)$ (A.95-A.96)

            Change limits β_{min} and β_{max} (A.97)

            Newton-Raphson (A.98)

            Calculate $eps = abs\left(\left(\beta_{new}-\beta\right)/\beta\right)$

            New overall fraction of vapor phase (A.100-A.101)

        Calculate liquid and vapour mole fractions (A.102-A.103)

    b) If the conditions A.89-A.90 are not met:

        Calculate liquid and vapour mole fractions (A.104-A.105)

    c) Call Algorithm B to obtain fugacity coefficients of the liquid and vapor phase

    d) Objective function (A.106)

    e) Calculate eps(TPN)

    f) Update K-factors from fugacity coeffcients (A.107)

END

3) Calculate VLE properties
}

Figure A6 Schematic representation of the TPn algorithm

1) **The Wilcom´s correlation is used to initialize the K-values (A.86)**

2) **WHILE (eps(TPN)<10^{-7}) THEN**

  Solve Rachford-Rice

    a. **Check conditions A.79-A.80 to know if there is a solution in the interval $\beta[0,1]$. If the conditions are met set $\beta_{min}=0$, $\beta_{max}=1$. If not, go to step 2.b.**

$$\sum_{i=1}^{C} z_i K_i - 1 > 0 \tag{A.89}$$

$$1 - \sum_{i=1}^{C} \frac{z_i}{K_i} < 0 \tag{A.90}$$

- **If $K_i > 1$ then**

$$\boldsymbol{\beta}_{\min} = max_i \left[0, \frac{K_i z_i - 1}{K_i - 1} \right] \qquad (A.91)$$

$$\beta_{max} = min_i \left[1, \frac{1 - z_i}{1 - K_i} \right] \qquad (A.92)$$

- **Calculate** $\beta_{ini} = 0.5(\beta_{min} + \beta_{max})$ $\qquad$ (A.93)

- **Change limits**

$$g(\beta_{ini}) > 0 \rightarrow \beta_{min} = \beta_{ini},$$
$$g(\beta_{ini}) < 0 \rightarrow \beta_{max} = \beta_{ini} \qquad (A.94)$$

- **WHILE (eps(Rachford-Rice) > 10^{-7}) then**

  o **Calculate** $g(\beta)$, $\boldsymbol{g'(\beta)}$
  $$g(\beta) = \sum_{i=1}^{C}(y_i - x_i) = \sum_{i=1}^{C} \frac{z_i(K_i - 1)}{1 - \beta + \beta K_i} = 0 \qquad (A.95)$$

  $$g'(\beta) = -\sum_{i=1}^{C} \frac{z_i(K_i - 1)^2}{(1 - \beta + \beta K_i)^2} < 0 \qquad (A.96)$$

  o **Change limits**
  $$g > 0 \rightarrow \beta_{min} = \beta,$$
  $$g < 0 \rightarrow \beta_{max} = \beta \qquad (A.97)$$

  o **Newton-Raphson**
  $$\Delta\beta = -\frac{g(\beta)}{dg/d\beta}$$
  $$\beta_{new} = \beta + \Delta\beta \qquad (A.98)$$

  o **Calculate eps**
  $$eps = abs\big((\beta_{new} - \beta)/\beta\big) \qquad (A.99)$$

  o **New overall fraction of vapor phase:**
  $$\beta = \beta_{new} \; if \; \beta_{new} \; is \; inside \; the \; interval \; [\beta_{min}, \beta_{max}] \qquad (A.100)$$

  o **If it is not, it is calculated as:**
  $$\beta = 0.5(\beta_{min} + \beta_{max}), \;\; \beta_{min} < \beta_{new} < \beta_{max} \qquad (A.101)$$

  o **Calculate liquid and vapour mole fractions**
  $$x_i = \frac{z_i}{1 - \beta + \beta K_i} \qquad (A.102)$$
  $$y_i = \frac{K_i z_i}{1 - \beta + \beta K_i} \qquad (A.103)$$

b. **If the conditions A.89-A.90 are not met [58]:**
If $\sum z_i / K_i \leq 1$ the liquid and vapour mole fractions are computed as:
$$\beta = 1$$
$$x_i = z_i / K_i$$
$$y_i = z_i \qquad (A.104)$$

1213	**Normalization of x_i**	
1214		
1215	**If $\sum z_i\, K_i \leq 1$ the liquid and vapour mole fractions are computed as:**	
1216	$\beta = 0$	
1217	$x_i = z_i$	
1218	$y_i = z_i * K_i$	(A.105)
1219	**Normalization of y_i**	
1220		
1221	c. **Call Algorithm B to obtain fugacity coefficients of the liquid and vapor**	
1222	**phase**	
1223	**Inputs**: Temperature, pressure, molar composition of the liquid or vapor	
1224		
1225	d. **Objective function**	
1226	$F_i = ln\varphi_v(T,p,y) - ln\varphi_l(T,p,x) + lnK_i = 0$	(A.106)
1227		
1228	e. **Calculate eps(TPN)**	
1229		
1230	f. **Update K-factors from fugacity coeffcients**	
1231	$K_i = exp(\, ln\varphi_l(T,p,x) - ln\varphi_v(T,p,y))$	(A.107)
1232		

3) Compute VLE properties

1235   a. **The phase fraction on mass ($\boldsymbol{\beta_m}$) basis is computed as:**

1237
$$\beta_m = \beta\, \frac{M_V (\text{mixture molar mass in liquid phase})}{M_T (\text{mixture molar mass})} \tag{A.108}$$

1239   b. **The equilibrium volume (v_{EQ}) is computed as:**

1240
$$v_{EQ} = \beta_m v_v + (1 - \beta_m)v_l \tag{A.109}$$

1242   c. **The equilibrium density is computed as:**

1243
$$\rho = \frac{1}{v_{EQ}} \tag{A.110}$$

1245   d. **The equilibrium internal energy is computed as:**

1246
$$e = \beta_m e_v + (1 - \beta_m)e_l \tag{A.111}$$

1248   e. **The equilibrium enthalpy is computed as:**

1249
$$h = \beta_m h_v + (1 - \beta_m)h_l \tag{A.112}$$

1251   f. **The speed of sound in the VLE state was computed using Wallis**
1252   **formula:**

1253
$$\frac{1}{\rho c_{wallis}^2} = \frac{\theta}{\rho_v c_v^2} + \frac{1 - \theta}{\rho_l c_l^2} \tag{A.113}$$

1255   **where the vapour volume fraction ($\boldsymbol{\theta}$) is computed as:**

1256
$$\theta = \frac{\rho - \rho_v}{\rho_v - \rho_l} \tag{A.114}$$

References

[1]   W. O. H. Mayer *et al.*, "Atomization and Breakup of Cryogenic Propellants Under High-Pressure Subcritical and Supercritical Conditions," *J. Propuls. Power*, vol. 14, no. 5, pp. 835–842, Sep. 1998.

[2]   C. Segal and S. A. Polikhov, "Subcritical to supercritical mixing," *Phys. Fluids*, 2008.

[3]   R. R. Rachedi, L. C. Crook, and P. E. Sojka, "An Experimental Study of Swirling Supercritical Hydrocarbon Fuel Jets," *J. Eng. Gas Turbines Power*, 2010.

[4]   B. Chehroudi, "Recent experimental efforts on high-pressure supercritical injection for liquid rockets and their implications," *International Journal of Aerospace Engineering*. 2012.

[5]   M. Oschwald *et al.*, "Injection of fluids into supercritical environments," *Combust. Sci. Technol.*, 2006.

[6]   R. N. Dahms, J. Manin, L. M. Pickett, and J. C. Oefelein, "Understanding high-pressure gas-liquid interface phenomena in Diesel engines," *Proc. Combust. Inst.*, 2013.

[7]   R. N. Dahms and J. C. Oefelein, "On the transition between two-phase and single-phase interface dynamics in multicomponent fluids at supercritical pressures," *Phys. Fluids*, vol. 25, no. 9, 2013.

[8]   J. Manin, M. Bardi, L. M. Pickett, R. N. Dahms, and J. C. Oefelein, "Microscopic investigation of the atomization and mixing processes of diesel sprays injected into high pressure and temperature environments," *Fuel*, vol. 134, pp. 531–543, 2014.

[9]   C. Crua, J. Manin, and L. M. Pickett, "On the transcritical mixing of fuels at diesel engine conditions," *Fuel*, vol. 208, pp. 535–548, 2017.

[10]   G. Mo and L. Qiao, "A molecular dynamics investigation of n-alkanes vaporizing into nitrogen: transition from subcritical to supercritical," *Combust. Flame*, vol. 176, pp. 60–71, 2017.

[11]   Y. Pei, E. R. Hawkes, S. Kook, G. M. Goldin, and T. Lu, "Modelling n -dodecane spray and combustion with the transported probability density function method," *Combust. Flame*, 2015.

[12]   Y. Pei *et al.*, "Large eddy simulation of a reacting spray flame with multiple realizations under compression ignition engine conditions," *Combust. Flame*, vol. 000, pp. 1–14, 2015.

[13]   M. Jangi, R. Solsjo, B. Johansson, and X. Bai, "International Journal of Heat and Fluid Flow On large eddy simulation of diesel spray for internal combustion engines," *Int. J. HEAT FLUID FLOW*, vol. 53, pp. 68–80, 2015.

[14]   L. Hakim, G. Lacaze, and J. Oefelein, "Large Eddy Simulation of Autoignition Transients in a Model Diesel Injector Configuration," 2016.

[15]   G. Lacaze, A. Misdariis, A. Ruiz, and J. C. Oefelein, "Analysis of high-pressure Diesel fuel injection processes using LES with real-fluid thermodynamics and transport," *Proc. Combust. Inst.*, 2015.

[16]   J. Matheis and S. Hickel, "Multi-component vapor-liquid equilibrium model for LES of high-pressure fuel injection and application to ECN Spray A," *Int. J. Multiph. Flow*, vol. 99, pp. 294–311, 2017.

[17]   J. Matheis and S. Hickel, "Multi-component vapor-liquid equilibrium model for LES and application to ECN Spray A," *arXiv Prepr. arXiv1609.08533*, 2016.

[18]   C. Rodriguez, P. Koukouvinis, and M. Gavaises, "Simulation of supercritical diesel jets using the PC-SAFT EoS," *J. Supercrit. Fluids*, vol. 145, pp. 48–65, Mar. 2019.

[19]   C. Rodriguez, A. Vidal, P. Koukouvinis, M. Gavaises, and M. A. McHugh, "Simulation of transcritical fluid jets using the PC-SAFT EoS," *J. Comput. Phys.*, vol. 374, pp. 444–468, Dec. 2018.

[20]   S.-K. Kim, H.-S. Choi, and Y. Kim, "Thermodynamic modeling based on a generalized cubic equation of state for kerosene/LOx rocket combustion," *Combust. Flame*, vol. 159, no. 3, pp. 1351–1365, 2012.

[21]   M. S. Wertheim, "Fluids with highly directional attractive forces. I. Statistical thermodynamics," *J. Stat. Phys.*, vol. 35, no. 1–2, pp. 19–34, Apr. 1984.

	[22]	M. S. Wertheim, "Fluids with highly directional attractive forces. II. Thermodynamic perturbation theory and integral equations," *J. Stat. Phys.*, vol. 35, no. 1–2, pp. 35–47, Apr. 1984.
1311		
1312		
1313		
1314	[23]	M. S. Wertheim, "Fluids with highly directional attractive forces. III. Multiple attraction sites," *J. Stat. Phys.*, vol. 42, no. 3–4, pp. 459–476, 1986.
1315		
1316	[24]	M. S. Wertheim, "Fluids with Highly Directional Attractive Forces . IV . Equilibrium Polymerization," vol. 42, pp. 477–492, 1986.
1317		
1318	[25]	W. G. Chapman, K. E. Gubbins, G. Jackson, and M. Radosz, "SAFT: Equation-of-state solution model for associating fluids," *Fluid Phase Equilib.*, vol. 52, no. C, pp. 31–38, Dec. 1989.
1319		
1320		
1321	[26]	W. G. Chapman, G. Jackson, and K. E. Gubbins, "Phase equilibria of associating fluids," *Mol. Phys.*, vol. 65, no. 5, pp. 1057–1079, Dec. 1988.
1322		
1323	[27]	N. Khare Prasad, "Predictive Modeling of Metal-Catalyzed Polyolefin Processes," 2003.
1324		
1325	[28]	S. Leekumjorn and K. Krejbjerg, "Phase behavior of reservoir fluids: Comparisons of PC-SAFT and cubic EOS simulations," *Fluid Phase Equilib.*, vol. 359, pp. 17–23, 2013.
1326		
1327	[29]	A. J. de Villiers, C. E. Schwarz, A. J. Burger, and G. M. Kontogeorgis, "Evaluation of the PC-SAFT, SAFT and CPA equations of state in predicting derivative properties of selected non-polar and hydrogen-bonding compounds," *Fluid Phase Equilib.*, vol. 338, pp. 1–15, 2013.
1328		
1329		
1330		
1331	[30]	M. Salimi and A. Bahramian, "The prediction of the speed of sound in hydrocarbon liquids and gases: The Peng-Robinson equation of state versus SAFT-BACK," *Pet. Sci. Technol.*, vol. 32, no. 4, pp. 409–417, 2014.
1332		
1333		
1334	[31]	K. S. Pedersen and C. H. Sørensen, "PC-SAFT Equation of State Applied to Petroleum Reservoir Fluids," *SPE Annu. Tech. Conf. Exhib.*, vol. 1, no. 4, pp. 1–10, 2007.
1335		
1336	[32]	P. C. Ma, L. Bravo, and M. Ihme, "Supercritical and transcritical real-fluid mixing in diesel engine applications," 2014, pp. 99–108.
1337		
1338	[33]	P. C. Ma, Y. Lv, and M. Ihme, "An entropy-stable hybrid scheme for simulations of transcritical real-fluid flows," *J. Comput. Phys.*, vol. 340, no. March, pp. 330–357, 2017.
1339		
1340	[34]	P. C. Ma, Y. Lv, and M. Ihme, "Numerical methods to prevent pressure oscillations in transcritical flows," no. 1999, pp. 1–12, 2017.
1341		
1342	[35]	R. W. Houim and K. K. Kuo, "A low-dissipation and time-accurate method for compressible multi-component flow with variable specific heat ratios," *J. Comput. Phys.*, vol. 230, no. 23, pp. 8527–8553, 2011.
1343		
1344		
1345	[36]	E. F. Toro, *Reimann Solvers and Numerical Methods for fluid dynamics*, vol. 40, no. 6. 2001.
1346		
1347	[37]	T. H. Chung, M. Ajlan, L. L. Lee, and K. E. Starling, "Generalized multiparameter correlation for nonpolar and polar fluid transport properties," *Ind. Eng. Chem. Res.*, vol. 27, no. 4, pp. 671–679, Apr. 1988.
1348		
1349		
1350	[38]	D. N. Justo-garcía, B. E. García-flores, and F. García-s, "Vapor - Liquid Equilibrium Data for the Nitrogen þ Dodecane System at Temperatures from (344 to 593) K and at Pressures up to 60 MPa," pp. 1555–1564, 2011.
1351		
1352		
1353	[39]	C. J. Mueller *et al.*, "Diesel Surrogate Fuels for Engine Testing and Chemical-Kinetic Modeling: Compositions and Properties," *Energy and Fuels*, vol. 30, no. 2, pp. 1445–1461, 2016.
1354		
1355		
1356	[40]	A. Vidal, C. Rodriguez, P. Koukouvinis, M. Gavaises, and M. A. Mchugh, "Modelling of Diesel fuel properties through its surrogates using Perturbed-Chain, Statistical Associating Fluid Theory."
1357		
1358		
1359	[41]	H. B. Rokni, A. Gupta, J. D. Moore, M. A. McHugh, B. A. Bamgbade, and M. Gavaises, "Purely predictive method for density, compressibility, and expansivity for hydrocarbon mixtures and diesel and jet fuels up to high temperatures and pressures," *Fuel*, vol. 236, no. August 2018, pp. 1377–1390, 2019.
1360		
1361		
1362		
1363	[42]	A. Tihic, G. M. Kontogeorgis, N. Von Solms, and M. L. Michelsen, "A predictive group-contribution simplified PC-SAFT equation of state: Application to polymer systems," *Ind. Eng. Chem. Res.*, 2008.
1364		
1365		

[43] R. K. Sinnott, *Coulson & Richardson's Chemical Enginering: Volume 6/Chemical Engineering Design*. Elsevier Butterworth Heinemann, 1999.

[44] M. L. Michelsen and J. Mollerup, *Thermodynamic Modelling: Fundamentals and Computational Aspects*. Tie-Line Publications, 2004.

[45] M. L. Michelsen, "THE ISOTHERMAL FLASH PROBLEM. PART I. STABILITY," *Fluid Phase Equilib.*, vol. 9, 1982.

[46] H. Hoteit and A. Firoozabadi, "Simple phase stability-testing algorithm in the reduction method," *AIChE J.*, 2006.

[47] N. Kyriazis, P. Koukouvinis, and M. Gavaises, "Numerical investigation of bubble dynamics using tabulated data," *Int. J. Multiph. Flow*, vol. 93, no. Supplement C, pp. 158–177, 2017.

[48] S. Kawai and H. Terashima, "A high-resolution scheme for compressible multicomponent flows with shock waves," *Int. J. Numer. Methods Fluids*, vol. 66, no. 10, pp. 1207–1225, Aug. 2011.

[49] H. Terashima and M. Koshi, "Approach for simulating gas-liquid-like flows under supercritical pressures using a high-order central differencing scheme," *J. Comput. Phys.*, vol. 231, no. 20, pp. 6907–6923, 2012.

[50] H. Terashima and M. Koshi, "Corrigendum to 'Approach for simulating gas-liquid-like flows under supercritical pressures using a high-order central differencing scheme' [J. Comput. Phys., 231, 20, (2012), 6907-6923]Doi: 10.1016/j.jcp.2012.06.021," *J. Comput. Phys.*, vol. 283, pp. 609–610, 2015.

[51] P. C. Ma, H. Wu, D. T. Banuti, and M. Ihme, "On the numerical behavior of diffuse-interface methods for transcritical real-fluids simulations," *Int. J. Multiph. Flow*, pp. 231–249, Apr. 2019.

[52] B. E. Poling, J. M. Prausnitz, J. P. O'connell, and others, *The properties of gases and liquids*, vol. 5. Mcgraw-hill New York, 2001.

[53] J. Gross and G. Sadowski, "Perturbed-Chain SAFT: An Equation of State Based on a Perturbation Theory for Chain Molecules," *Ind. Eng. Chem. Res.*, vol. 40, no. 4, pp. 1244–1260, 2001.

[54] M. Farzaneh-Gord, M. Roozbahani, H. R. Rahbari, and S. J. Haghighat Hosseini, "Modeling thermodynamic properties of natural gas mixtures using perturbed-chain statistical associating fluid theory," *Russ. J. Appl. Chem.*, vol. 86, no. 6, pp. 867–878, 2013.

[55] N. Diamantonis and I. Economou, "Evaluation of SAFT and PC-SAFT EoS for the calculation of thermodynamic derivative properties of fluids related to carbon capture and sequestration," no. June 2011, pp. 1–32, 2011.

[56] B. E. Poling, *The properties of gases and liquids / Bruce E. Poling, John M. Praausnitz, John P. O'Connell*. 2001.

[57] R. Privat, R. Gani, and J. N. Jaubert, "Are safe results obtained when the PC-SAFT equation of state is applied to ordinary pure chemicals?," *Fluid Phase Equilib.*, vol. 295, no. 1, pp. 76–92, 2010.

[58] E. Scientific, P. Company, and L. Michelsen, "The isothermal flash problem. part ii. phase-split calculation," vol. 9, 1982.